ARCTIC SEA ICE: THE DEVELOPMENT OF A 3-D MODEL FOR ENHANCED SUBSURFACE STORAGE CAPACITY CALCULATIONS

By

Kelsey A. Frazier, B.A.

A Thesis Submitted in Partial Fulfillment of the Requirements

for the Degree of

MASTER OF SCIENCE

in

Mechanical Engineering

University of Alaska Anchorage

December 2019

APPROVED:

Getu Hailu, Ph.D., Committee Chair
Jennifer Brock, Ph.D., Committee Member
Larry Morris Foster, Ph.D., Committee Member
Jifeng Peng, Ph.D., Chair
Department of Mechanical Engineering
Jennifer Brock, Ph.D., Interim Associate Dean for Academics
Department of Mechanical Engineering
John Stalvey, Ph.D., Interim Provost & Acting Dean
Graduate School

Abstract

In the event of an Arctic oil spill, ice in the water is a complicating factor. The presence of ice complicates the forecasting of the movement and spreading of oil as well as the planning of the oil spill clean-up process. The underside of Arctic sea ice is not flat, rather it presents non-geometric, unpredictable protrusions into the water column. The depth to which these protrusions grow relates to the longevity of the ice itself. The challenge faced by the oil spill forecaster is that information on the under-ice storage capacity is not readily available. Previous work explored how to estimate under-ice storage capacity based on ice stage. This thesis expands that work, investigating the translation of a two-dimensional model into three dimensions.

Historical reports on Arctic sea ice stage (e.g., first year, thin ice) were obtained from the Alaska Ocean Observing System. Next, historic data was acquired on draft measurements. During the winters of 2005-2013, Shell deployed upward looking sonar at several sites in the Beaufort and Chukchi Seas. The sonar made direct measurements of ice draft. The under-ice storage capacity, defined as the volume of pore space above the average ice draft level, was estimated based on the ice draft data. Concentrating in on that data, older, first year ice draft measurements extracted and further analyzed.

Analyzing the ice draft, it was determined that drafts follow a negative exponential distribution. That information allowed the construct of an array following the same distribution and data mean. Modeling that array in ArcGIS provided the necessary framework from which to compute storage capacity in three dimensions. This calculation followed the previous work. While the two-dimensional model suggested a storage capacity ranging from 15,000 to 50,000 m^3/km^2, the three-dimensional model produced a capacity on the order of 415,991 m^3/km^2. It is proposed that the 2-D storage capacity calculation, when extended into 3-D, overestimates the total ice volume for an area, thus depressing the total storage capacity volume. Discussion follows on need for further exploration of the subject.

Table of Contents

Page

Title Page i

Table of Contents v

List of Figures vii

List of Tables ix

List of Appendices xi

Acknowledgments xiii

1 Introduction 1

2 Prior Work 3

2.2 2-D Model Criticism 9

3 Objective 11

4 Literature Review 13

4.1 Sea Ice Growth 13

4.2 Boundary Layers 14

4.4 Threshold Velocity 18

4.5 Roughness 19

4.6 Draft Distributions 22

4.7 Subsurface Volume 26

5 Methodology 29

5.1 Draft Data 29

5.3 MATLAB Analysis 31

5.4 Statistical Analysis 32

5.4.1. Histogram 32

5.4.2 Central Tendency 36

5.4.3. Distribution Fitting 37

5.5 Goodness-of-Fit 40

5.6 Data Generation 41

6 Discussion 45

7 Future Work 49

References 51

Appendices 55

List of Figures

Page

Figure 1. WMO ice "egg code" illustration 4
Figure 2. 2-D model schematic of the underside of sea ice. 7
Figure 3. Sea ice subsurface storage capacity compared to observed ice surface stage. 8
Figure 4. Regional mean sea ice draft and composition for Beaufort and Chukchi Seas. 24
Figure 5. An example of an ice ridge cross section. 24
Figure 6. Probability denisty of mean keel area coefficient. 25
Figure 7. Semi-log scale of sea-ice draft probability density function. 25
Figure 8. General locations (in red) of Shell data collection sites. 29
Figure 9. Schematic of the moorings for IPS (left) and ADCP (right). 30
Figure 10. Ice condition '7,10,12' histogram with 100 bins. 32
Figure 11. Ice condition ‘7,10,12’ histogram with 1000 bins. 33
Figure 12. Draft measurements less than 0.5 m. 34
Figure 13. Draft measurements between 0.5 and 1.4 m. 35
Figure 14. Draft measurements greater than 1.4 m. 35
Figure 15. Comparison of the mode, arithmetic, and geometric means. 36
Figure 16. Distribution fitting for draft data. 38
Figure 17. Probability plot for data compared to various distributions. 39
Figure 18. Linearized exponential CDF plot. 40
Figure 19. Raster image with contour overlay for surface ice condition 43
Figure 20. The subsurface of the sea ice is modeled in ArcGIS, upside down, for illustration. 44
Figure 21. 2-D draft heights linearly extrapolated over a 3-D domain. 46
Figure 22. Side scan sonar imaging of a pressure ridge. 48

List of Tables

Page

Table 1. Ice "egg code" used to define ice stage..... 5
Table 2. Summary of ice-ocean drag coefficients, Cw. 21
Table 3. Regional spring and autumn mean and modal draft. 23
Table 4. Summary of potential pooling volume for oil released beneath fast ice. 27
Table 5. Test statistics from the Chi-square test. 41

List of Appendices

Page

Appendix A Beaufort Surface Data 55

Appendix B Chukchi Surface Data 59

Appendix C Matlab Code for Draft Measurements 63

Appendix D Distribution Fitting Data 69

Appendix E Matlab Draft Creation 71

Appendix F ArcGIS Data 73

Acknowledgments

No educational pursuit is solely accomplished by the individual student. It takes a community, a tribe, and a family to see the student through to the end. In that, I am no different.

I'd like to thank the community that has supported me more decades that I'd like to count. Thank you to BP who sponsored my tuition and introduced me to the unique engineering opportunities, and challenges, in the energy sector. Thank you to BP Exploration Alaska who, by my account, has been sponsoring my education, in one way or another, since kindergarten. In the last few years you took me in as an intern and produced a more confident, competent engineer on the other end. We will miss your presence in Alaska, but you've left us with a legacy of safety, respect, and one team!

My tribe is a bit more varied. Thank you to the staff of the Arctic Domain Awareness Center, who have been my cheerleaders and colleagues the last 4 years. You rarely told me 'no' when I pitched a research idea or wanted to take on a project. Your patience and encouragement overwhelm me. To the "Three Amigos," Dean Kamen, Woodie Flowers, and Dave Lavery: I am proof of concept albeit twenty years in the making. Thank you for lighting the fire that never died, and for saving me from the edge more times than I can count. I'll be defending this thesis in denim in your honor (I'm saving the tux for the Ph.D., Woodie). And to all the friends (Dave P., Kathi A., Tom R., Kim P., Cathleen C., Linda H., and Aimee D.) who have put up with my whining, moaning, complaining, and generally grumpy demeanor . . . thank you for ample amounts of coffee, wine, pedicures, chocolate, and hugs. Oh, and the listening, definitely thanks for the listening!

To my family whom I'm surprised hasn't deleted my phone number and blocked my calls. Thank you to my parents who helped with organizing food, errands, childcare, travel, etc. I would never have been able to finish my master's degree without you. Or that pesky undergrad degree. Finally, to my son, Thomas, thank you for telling me it'd be okay when the stress made me cry; for telling me that this degree would be worth it in the end. You are wise beyond your years.

1 Introduction

On August 11, 1778, Captain James Cook sailed through the Bering Strait in search of the rumored northwest passage (ARCUS, 2019). Instead of finding the fabled waterway connecting the Atlantic and Pacific oceans, the expedition was confronted with ice walls soaring ten to twelve feet above the surface of the water. These ice walls stretched across the strait and blocked all progress north. Since those accounts, ice has been ubiquitous with the Arctic, shaping society's views of the inhospitable nature of the region. In the last 30 years, however, regional changes in climate have significantly altered the nature of ice in the Arctic Ocean.

Today, it is common to have four or five months of open water surrounding the northern shoreline of Alaska on the Arctic Ocean. Periods of freezing are trending later in the year, and thawing occurs earlier. Ice that has stayed frozen year-round for more than one season, called multi-year ice, has retreated to the very center of the ocean. Now, most of the sea ice averages a few feet thick over the course of an entire season. This reduction in the length of ice presence and the thickness of the ice has led to increased coastal erosion and underwater permafrost melting, negatively impacting coastal structures and communities. In that same vein, though, the retreat of sea ice has also led to new economic opportunities.

Retreating sea ice has opened up lanes for commercial and private endeavors in the Arctic. In 2013, the Nordic Orion carried coal from Vancouver, Canada to Finland through the Northwest Passage (Waldie, 2014). This route bypassed the Panama Canal, and was 2500 miles shorter between ports. In 2016, Crystal cruises sent a passenger ship, the Crystal Serenity, on a thirty-two-day voyage through the Arctic, along the coasts of Alaska and Canada (Nunez, 2016). Since this activity, there has been tremendous development in building Arctic capable ships by China and Russia with the intent to utilize the Arctic Ocean for shipping.

Resource development in the Arctic is another area of interest to Arctic nation states and commercial enterprise. Oil and gas extraction from the sea floor in the U.S. Exclusive Economic Zone (EEZ) has been explored by Shell and Statoil off the northern coast of Alaska. Underwater mineral mining has also been proposed. Operating in the Arctic does come with certain risks, though. While the ice is retreating, it is still present in the water for many months. The wind and current move that ice, which threatens vessels. Ice can also penetrate deep into the water column,

forming drafts, which can scour the sea floor, threatening submarine pipelines. Further, bathymetric surveys of the ocean floor are outdated and unmapped physical hazards may be hidden beneath the surface. The last comprehensive bathymetric survey was completed when Abraham Lincoln was the seated President.

As traffic increases in the Arctic, so too does the need to understand the complex dynamics of the ice and its surroundings. In particular, the Arctic is most at risk should an Arctic oil spill occur. This spill might take the form of an accidental release of crude oil from a subsurface pipeline rupture, or a surface release of diesel from a ship collision or grounding. In any case, the presence of ice complicates the ability of first responders to contain and clean up oil on the water's surface. Prolonged exposure to the environment of a contaminant endanger not only the local marine life, but the communities that depend on that marine life for food as well. Some contamination, once grounded on the shoreline, could seep into the soil and remain for decades. Therefore, it is crucial to properly model the interaction between oil and sea ice to better anticipate Arctic oil spill slick spreading.

2 Prior Work

The National Oceanic and Atmospheric Administration (NOAA) operates an oil spill model referred to as the General NOAA Operational Modeling Environment (GNOME). Until relatively recently, GNOME did not account for the influence of sea ice and its influence on oil slick spreading (Zelenke et al. 2012). However, the recent interest in Arctic resource exploration has made the development of an Arctic-capable GNOME model imperative.

Thesis work by Dana Brunswick at the University of Alaska Anchorage, under the guidance of Dr. Tom Ravens, University of Alaska Anchorage, and Dr. Scott Socolofsky, Texas A&M University, led to the development of an updated Arctic-capable GNOME model with sea ice inputs. Currently, the model can account for the weathering and motion of oil in the water with partial ice cover, but not full ice cover.

Total ice cover and the roughness of the ice subsurface influence oil slick motion. When sea ice covers less than 70% of the water's surface, the dominant mover of oil is the current. For cover greater than 70%, oil is moved by the ice. Further complicating the issue, if sea ice is relatively flat on the subsurface, the oil moves with the current beneath the ice. When the ice is not smooth but forms complicated geometries protruding into the water column, the oil moves in relation to the ice motion. Therefore, it is critical to understand the subsurface shape of the ice for proper oil slick modeling.

In a previous project (Frazier & Ravens, 2019), a paper was published on the under-ice storage capacity of sea ice. A relationship between observable surface conditions and subsurface storage space was drawn. Draft data provided the 2-D subsurface inputs from which the storage space was calculated. Based on these calculations, a rough range of storage capacity was proposed.

2.1 The 2-D Model

To develop the range of storage capacities beneath sea ice, in relation to the surface conditions, the project utilized ice data from the U.S. National Ice Center (NIC). Here, multiple data sets from the POES and GOES satellites are interpreted and a daily report is produced regarding ice conditions and concentrations for all US waters in the Arctic. This report

communicates ice conditions in different Arctic regions through an ice “egg code,” like that in Figure 1 (WMO, 1970).

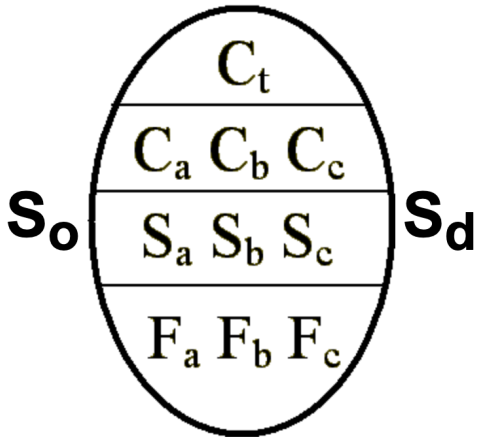

Figure 1. WMO ice "egg code" illustration

The egg code, named for its unique reporting shape, offers a convenient coding scheme which was developed by the World Meteorological Organization (WMO, 1970). This scheme reports the total concentration of ice cover (C_t) at the top of the egg for a given area. Moving down the egg, the second line lists the partial concentrations ($C_{a,b,c}$) of sea ice in order of decreasing thicknesses (a being the most thick, c being the least thick), the third line lists the stages of development of the sea ice ($S_{a,b,c}$, a being most developed, c being least developed), and the bottom of the egg lists the predominant form of the sea ice, or ice floe size ($F_{a,b,c,}$ a being the largest size, and c being the smallest size). The remaining development stages, or the age of the remaining sea ice types, are reported on the outside of the egg, noted as S_o for trace amounts of sea ice, and S_d for thinner sea ice. These extraneous categories are used when there is an unusual sea ice presence or composition in the area.

This code for $C_{a,b,c}$ is illustrated in Table 1, where potential values for C on the egg might be reported. A typical egg might report $C_{a,b,c}$ as ‘ 7 4 1’ for a particular region, communicating that the thickest ice observed is 30-70 cm thick, then the next thickest ice is 15-30 cm thick ice, and finally, the least thick ice is 0-10 cm thick. $S_{a,b,c}$ and $F_{a,b,c}$ follow similar schemes but are not illustrated here as those values were not used in this thesis.

Table 1. Ice "egg code" used to define ice stage

Ice Egg Code	1	2	3	4	5	6	7
Modified Code	1	2	3	4	5	6	7
Thickness (cm)	0-10	10-30.	10-15.	15-30.	15-30.	30-200.	30-70.
Description:	New, Frazil, Slush, etc	Nilas, Ice Rind	Young	Gray	Gray - White	1Y	1Y, Thin
Ice Egg Code	8	9	1*	4*	7*	8*	9*
Modified Code	8	9	10	11	12	13	14
Thickness (cm)	30-70.	30-70.	70-120.	>120	>2m	>2m	>2m
Description:	1Y, Thin, Stage 1	1Y, Thin, Stage 2	1Y Ice, Medium	1Y Ice, Thick	Old 1Y Ice	SY Ice	MY Ice

Egg codes for the 2-D model were obtained through the Arctic Ocean Observing System (AOOS) and it was noted that a majority of the historic data differed from convention, as numerous samples did not provide stage (Figure 1, line 3) in order of decreasing thickness. Rather, the code has historically provided the code in order of greatest areal coverage of a given thickness (C_a), then the second most prevalent areal coverage of ice thickness (C_b), followed by the smallest areal coverage of ice at a third thickness (C_c). This code might appear as '7,3,10,' for example. However, the egg code provided the foundation from which a relationship between the surface and subsurface was developed. To achieve an under-ice storage capacity estimation, the project investigated how well the observed ice condition reports correlated with a measured under-ice storage capacity.

The ice stage above each ADCP/IPS data point during the 2010-2013 measurement period was obtained from AOOS. Ice stage data was available in the form of the ice egg code (described above) and was available on a weekly basis. The code includes fourteen ice stage designations. This project converted ice stage at a given location and time into a single, comma separated identifier, such as '1,3,7' or '10,11,12'. Modifications to the reported WMO standard egg code were made so that data could be sorted in Excel. The relationship between the standard code and the modified code is listed in rows one and two of Table 1.

Sea ice is characterized by sub-surface roughness. This roughness ranges from slight impressions to large cavities formed between drafts (Wadhams et al. 2006, Rothrock and Thorndike 1980). Multi-year ice tends to have greater roughness than first year ice (Comfort and Purves 1982, Kovacs 1977). The roughness of the subsurface of sea ice influences how an oil slick will spread in ice covered water. Oil, being buoyant, will fill the cavities in the underside of the ice (Venkatesh et al 1990).

Glaeser and Vance (1971) studied this phenomenon using several small-scale releases of crude oil beneath pack ice in the Chukchi Sea. They noted that oil under the ice did not spread if sufficient storage space was available in these "void" spaces. When the storage space was filled, the oil spilled over into adjacent spaces. While buoyant, viscous, and surface tension forces also play a role in subsurface spreading, Fingas and Hollbone (2003), and Afenyo et al. (2016), describe under ice topography as one of the dominant factors in determining slick spread. Hence, in order to be able to predict the spreading of oil under ice, it is important to quantify the under-ice storage capacity based on under-ice topography.

While under-ice storage capacity has a known influence in Arctic oil spill modeling, there was some question in related literature as to how to define a storage variable. There was effort by Puskas et al. (1987) to quantify roughness in their equations for determining oil slick thickness. They associated storage capacity with hydraulic roughness, but this roughness acted more as a correction factor and was assumed to be spatially constant. From direct observation, Arctic sea ice void space grows and wanes during the winter season. As those spaces change, the storage capacity too will change. A better descriptor is the relationship developed by LeSchack and Chang (1977) relating the RMS ice draft to potential storage capacity (Equation 1). The 2-D model used that definition for the under-ice storage capacity as the void space above the time average ice draft level (Figure 2).

$$\delta_{sc} = \frac{\iint \left((h'_{ice} > h_{mean}) - h_{mean} \right) \, dx \, dy}{A_d} \tag{1}$$

Where,

δ_{sc} = Storage capacity of the ice (m^3/km^2),

h_{mean} = mean ice draft over a given length (m),

h'_{ice} = ice draft at a position at (x,y) (m),

and A_d = domain area of ice surface (km^2).

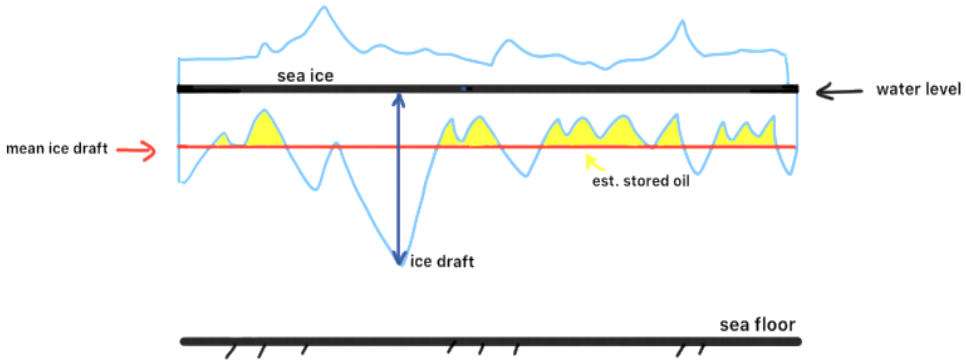

Figure 2. 2-D model schematic of the underside of sea ice.

Computed weekly subsurface storage capacity estimations, in combination with the associated surface condition ice egg condition, are graphed in Figure 3. When sorted by increasing stage of the thickest fraction of the ice, a distinct trend in the data can be identified. Generally, as the ice ages, storage capacity increases. There does appear to be a maximum capacity which develops, after which, subsurface storage capacity declines. Fast ice, or ice that was connected to the land, generally develops later in the season but its relative storage capacity was low. That type of ice may experience subsurface smoothing by the current due to its stationary nature.

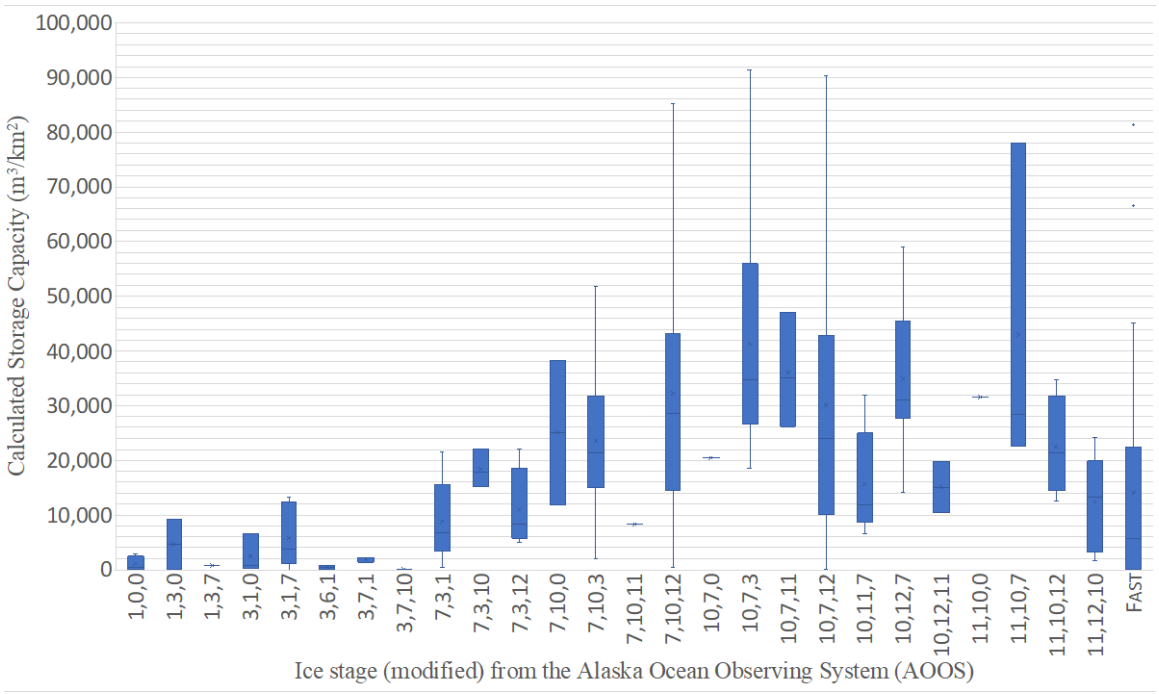

Figure 3. Sea ice subsurface storage capacity compared to observed ice surface stage.

Weekly estimations that significantly over or under-estimated storage capacity were excluded from the results. Excluded data included sets that produced a large storage capacity in relatively new or melting ice, which occurs when the battery in the IPS gets weak and the system malfunctions. Ice draft measurements that were taken under ice that appeared to hover over the same area was also excluded. Those measurements would have erroneously skewed the storage capacity estimation when converted to a spatial data series. Additionally, the weekly periods for which ice draft was calculated, and surface conditions were reported, did not always align, often separated by two or three days. Over the three-year sample period, 183 capacity calculations were considered "valid" from which to draw a relationship.

It is noted that some of the ice stages have particularly long whiskers for their particular box and whisker plots, especially for the '7,10,3,' '7,10,12,' and '10,7,12' categories. Those whiskers indicate the upper and lower extremes in the calculated storage capacities, from outliers in the data. These outliers signify that the filtering techniques for the raw data did not work well enough in these categories.

From the graphical analysis in Figure 3, oil storage capacity beneath sea ice was estimated on a low, medium, and high spectrum, which appears to be positively correlated to the

stage of the thick ice fraction present. When the ice stage of the thickest ice fraction was assigned an ice egg code of 1 or 3 (Table 1), storage capacity was 'low,' identified by less than 15,000 m^3/km^2 of void space. For a primary ice stage with a 7 or 10, storage capacity was 'medium,' between 15,000 and 50,000 m^3/km^2. Older ice with an ice egg code of 11 or greater has a 'high' storage capacity of 50,000 to 80,000 m^3/km^2.

2.2 2-D Model Criticism

While the 2-D model was an adequate first effort to quantify sea ice subsurface storage capacity, there are some drawbacks to the approach. First, the work evaluated volumetric storage capacity based on a two-dimensional data set. A mean draft was computed from the weekly draft data measurements, above which the storage area was calculated. Then the two-dimensional void space was extended linearly across a one-kilometer distance. Geometrically, this would look like huge troughs gouged into the sea ice and it has not been verified whether this is (a) an accurate representation of the subsurface, or (b) an approximate representation of the subsurface.

Second, there was little work beyond LeSchack and Chang (1977) to validate whether the mean draft as the threshold above which storage space is calculated was a reasonable measure of how much oil could pool before the current, ice, or both, moved the oil away. The dynamic nature of the ice-water interface for rough surfaces is poorly understood. Proper modeling of the ice subsurface will assist in determining whether LeSchack and Chang's definition is appropriate, or if their definition is an oversimplification of a possible pooling profile.

3 Objective

Given the relative uncertainty of extrapolating a two-dimensional space into a three-dimensional volume, the objective of this project is to better establish sea ice subsurface storage capacity. As the presence of multiyear sea ice declines in the Arctic Ocean, first year ice will become the dominant observed condition. Due to this changing nature of the Arctic, and the need for enhanced understanding of the subsurface of sea ice, this project will advance the definition of "storage capacity" by modeling the ice subsurface in three dimensions.

Specifically, this project models the subsurface of sea ice correlating to a modified ice egg condition of 7,10,12. Draft data is analyzed statistically, extrapolated over a 3-D grid, and used to build a surface model in ArcGIS. Further testing of the current definition of "storage capacity" is done within the ArcGIS model by changing the relative pooling depth at the water-ice interface and computing a total stored volume. Finally, the results of the model are compared to the results of the 2-D model, followed by a discussion of the relative accuracy of LeSchack and Chang's 1977 definition of storage capacity in literature.

4 Literature Review

4.1 Sea Ice Growth

Drift, or pack ice, which isn't attached to land, is typified by an irregular subsurface. Unlike lake ice cover, which grows without the influence of waves, tides, and currents, sea ice grows in a turbulent environment. When external environmental factors aren't present, ice grows downward at a rate dependent upon the ongoing rate of heat flux, $\dot{Q}$, at the ice-water interface. Assuming local thermal equilibrium, and measurable environmental parameters, heat transfer is solved using the linearized form of Fourier's Law (Equation 2).

$$\dot{Q} = -kA\frac{(T_s - T_w)}{\Delta x} \tag{2}$$

Where,

k is the thermal conductivity $\left(\frac{W}{m*K}\right)$

A is the surface area of the interface between water and ice (m^2)

T_s is the surface temperature (K)

T_w is the water temperature and assumed to be at or near the freezing point (K)

Δx is ice thickness (m, assumed to be known), and

$\dot{Q}$ is found in units of (W).

When the downward growth profile is combined with turbulent surface forces, sea ice develops into discontinuous floes. Motion of the floe depends on the forcing mechanism present, such as tides, currents, and wind. Once that ice floe reaches exceeds a certain size, the floe momentum is high enough to resist the external forces applied by the surrounding water and is moved to a larger extent by the prevailing wind (Thorndike and Colony, 1982; Hilmer et al., 1998). Wind drives floes to converge, causing compression and shearing at the floe interface (Steiner, Harder & Lemke, 1999). The reaction to this work by the wind on the floe is the creation of pressure ridges, generalized plastic deformation, and friction (Rothrock, 1975).

Pressure ridges and plastic deformation influence the “roughness” characteristic of the subsurface.

4.2 Boundary Layers

A simplifying assumption frequently employed in classical fluid dynamics is that flows are inviscid, i.e. that fluid drag is negligible and can be discounted. This assumption is not appropriate for this model, which examines the ice-water interface. At solid-fluid interfaces, viscous forces are considerable and lead to the formation of boundary layers within the fluid. For that reason, viscous resistance at the solid-liquid interface is critical to the understanding, and quantification of, subsurface roughness.

On the scale of a water molecule, even a finely machined surface would “look” rough, and the surface of smooth ice even rougher. As water molecules encounter the ice boundary, they collide with the numerous peaks and valleys on the surface, not to mention other neighboring molecules. The exchange transfers both momentum and thermal energy with the surface. The more pronounced the surface roughness, the greater the momentum, and thermal, exchange.

The importance of viscous resistance and energy exchange at an interface leads to a discussion of boundary layer theory. The concept of a boundary layer was proposed by Prandtl in 1904 to better quantify observable drag effects often ignored due to their complexity in the Navier-Stokes equations (Schetz, 1984). Assuming high-Reynolds number flow, Prandtl surmised that viscous effects would be confined to a thin layer along the boundary between two surfaces. Within this boundary, large velocity gradients lead to large shear forces even for low viscosity fluids. All momentum, heat, and mass transfer to or from the surface occurs within this boundary layer. Outside the boundary, viscous effects are negligible and the flow may be treated as if inviscid.

The profile of the velocity within this boundary layer is characterized by both the wall shear force applied to the fluid, and the density of the fluid itself. This relationship is illustrated in Equation 3, and described as the friction velocity, u_* (Schetz, 1984).

$$u_* \equiv \sqrt{\frac{\tau_w}{\rho}}, \left(\frac{m}{s}\right) \tag{3}$$

Where,

τ_w is the wall shear (Pa), and

ρ is the fluid density (kg/m^3).

The friction velocity is related to the skin friction drag coefficient, C_f, defined by Equation 4 (Schetz, 1984).

$$C_f = \frac{\tau_w}{\frac{1}{2}\rho U_e^2} \tag{4}$$

And U_e is the velocity at the outer edge of the boundary layer. Solving for the shear force at the wall, and substituting, Equations 3 and 4 are shown to be related by Equation 5 (Schetz, 1984).

$$\frac{u_*}{U_e} = \sqrt{\frac{\tau_w}{\rho U_e^2}} = \sqrt{\frac{C_f}{2}} \tag{5}$$

This relationship makes a critical point in the potential behavior of oil particles within the boundary layer. If the boundary layer could be held at a uniform thickness, as the flow encounters areas of higher roughness, the velocity of that fluid increases downward. At the underside of an ice floe, this behavior acts such that fluid moves normal to the ice surface, dragging oil droplets away from the surface.

Boufadel, Cui, Katz, Nedwed and Lee (2018) numerically investigated the relationship between oil particle motion and the boundary layer at the water-ice interface. They were specifically concerned with the affect the boundary layer had on particle velocity and eddy diffusivity, and how that related to the attachment efficiency of the oil to the ice wall. It was theorized that if oil particles are less capable of attaching to the ice wall, then they are more likely to be swept away by the current.

As the boundary layer in their model expanded and contracted, due to the presence of changing surface roughness, the gradient of the eddy diffusivity also changed (Boufadel, Cui, Katz, Nedwed and Lee, 2018). Eddy diffusivity affects the vertical transport of oil droplets within a boundary layer. The greater the diffusion coefficient, the greater the vertical motion of the particles and the less likely they are to congregate near the ice surface.

It would seem that subsurface ice roughness, then, encourages transport of molecules away from the surface. Boufadel et. al. found that most oil spill models ignored the relative changes in the eddy diffusivity gradient and showed through their own model the deleterious effects of ignoring this gradient. Ignoring the boundary means ignoring the frictional drag caused by the ice surface and leads to an under-estimation of the speed at which a slick can spread.

Conversely, what the Boufadel et. al. work ignored was the influence of the thermal gradient. Convective heat transfer would alter the energy balance within the boundary layer and may lead to lower diffusivity. Further, while they recognized that a boundary layer in real situations cannot grow to infinite depths, the researchers chose to base their calculations on a boundary layer thickness by McPhee and Smith (1976). McPhee and Smith measured the purported boundary layer beneath Arctic sea ice, which they claim is between 2.0 and 6.0 m deep. Upon review, the evidence for this claim is scientifically lean. Finally, Boufadel et. al. did not account for the salinity gradient present at an ocean-ice interface. When sea ice grows, it expels salt, creating a thin layer of highly concentrated saltwater. The saltwater layer may act as another boundary for oil particles, and the interaction should be more closely investigated.

4.3 Oil Slick Spreading

The thickness of an oil slick beneath ice is influenced by buoyancy, surface tension and gravitational forces. If sufficient external forces exist, the slick remains thin and reaches further in-plane. When the viscosity of the fluid dominates, significant ice pooling occurs. However, spreading is generally recognized as an important component of oil spill modeling in the time immediately following the release; transport from advection and turbulence provide most movement later on. (Glaeser & Vance, 1971)

In 1975, Hoult et al used the work of Fay (1969), with oil slick spreading in open water, to explore spreading beneath sea ice. He proposed pressure differentials as the dominant force

influencing slick motion. Spreading oil that encounters a void space will experience a drop in localized pressure, slowing the overall motion. As sea ice roughness increases, oil slick spreading should reduce. Equation 6 describes the radius of an oil slick beneath ice as a function of subsurface roughness leading to a pressure change (Hoult, Wolfe, O'Dea, & Patureau, 1975).

$$r = 0.25\left(\left(\frac{\rho_{water}}{\rho_{oil}} - 1\right)\frac{gQ^2}{h'_{ice}}\right)^{1/6} t^{2/3} \quad (6)$$

Where,

r is the radius of the oil slick (m),

Q is the volumetric flow rate of the oil (m^3/s),

g is acceleration due to gravity (m/s^2),

h'_{ice} is half of the root mean square roughness height of the ice cover,

ρ_{water} and ρ_{oil} are the densities of water and oil respectively (kg/m^3),

and t is the time from oil release (s).

This equation was validated using laboratory experiments with artificial ice in a flume and kerosene released beneath the surface.

Later, Yapa and Chowdhury (1990) developed a means of describing oil slick spreading from a simplified Navier-Stokes equation. Spreading is calculated as a balance between interfacial tensions between ice-water, oil-water, and oil-ice surfaces. Buoyancy forces dominate, followed by a buoyancy-inertia phase (Equation 7), then a buoyancy-viscous phase (Equation 8). The final radius of the slick (Equation 9). Once the slick is sufficiently thin, interfacial tension is the primary driver of spreading (Yapa & Chowdhury, 1990).

$$r = 0.751\left(\left(\frac{\rho_{water}}{\rho_{oil}} - 1\right) gQ\right)^{1/4} t^{3/4} \quad (7)$$

$$r = k_{yc1}\left[\frac{(\rho_{water} - \rho_{oil})gQ^3}{\mu_{oil}}\right]^{1/8} t^{1/2} \; (Q = constant) \quad (8)$$

$$r = k_{yc2}\left[\frac{(\rho_{water} - \rho_{oil})gV^3}{\mu_{oil}}\right]^{1/8} t^{1/8} \; (V = constant)$$

$$r_f = k_{yc3}\left[\frac{g(\rho_{water}-\rho_{oil})}{\sigma_n}\right]^{1/4} V^{1/2} \quad (9)$$

Where,

r is the radius of the oil slick (m),

r_f is the final radius of the oil slick (m),

Q is the volumetric flow rate of the oil (m^3/s),

g is acceleration due to gravity (m/s^2),

ρ_{water} and ρ_{oil} are the densities of water and oil respectively (kg/m^3),

t is the time from oil release (s),

k_{yc1}, k_{yc2}, k_{yc3} are dimensionless constants,

μ_{oil} is the dynamic density of the oil (Pa),

V is the volume of oil spilled ($\pi R^2 h$),

h is the mean thickness of the slick (m),

$and\ \sigma_n$ is the net interfacial tension (N/m).

Yapa and Chowdhury (1990) verified their equations in laboratory experiments. These experiments used a variety of oils with different viscosities, and what they identified as "smooth" and "rough" ice. The found that upon release, oil tends to separate into small particles between 0.1 and 2.0 cm in diameter. They attributed this separation to an imbalance in the surface tension of the oil surface, and the buoyancy of the particles stimulated motion toward the ice-water interface.

4.4 Threshold Velocity

The sinking of the vessel "Runner 4" in the Gulf of Finland in 2006 allowed for the collection of oil spill slick spreading data in water with high concentrations of ice. This data was used to validate improvements for oil-in-ice parameters implemented in the Seatrack Web oil spill model employed by agencies in Finland, Sweden, and Denmark. One of the tests was to evaluate the model sensitivity to a constant threshold velocity. The threshold velocity describes

the velocity at which oil beneath ice is swept away, typically cited as 0.2 m/s (Cox & Schultz, 1981; Arneborg et al., 2017).

The study found that the mean trajectory of the oil slick output by the model was highly sensitive to the threshold velocity. Neither the original model nor the improved model was one hundred percent accurate, though the new parameters with the new threshold velocity more closely followed the observed oil slick path. The model movement moved more slowly, on a scale of approximately three days, than the observed movement. Researchers attribute the challenge of accurately addressing the timing of the slick motion to a lack of knowledge regarding velocity thresholds and the relationship they have to under ice roughness.

4.5 Roughness

Characterizing the subsurface roughness of sea ice is important in many areas of Arctic research. Examples include determining sea ice thicknesses for large-scale Arctic ice models (Maslowski & Lipscomb, 2003), assessing sea ice loads on offshore structures and ice-capable vessels (Timco & Weeks, 2010), quantifying wind and water drag coefficients for dynamic modeling (e.g., Andreas, Lange, Ackley & Wadhams, 1993), and the confinement of oil spills under ice (Wilkinson, Wadhams & Hughes, 2007).

The first mention of a method for quantifying ice subsurface roughness comes from LeSchack and Chang (1977) in their analysis of submarine sea-ice draft measurements from Arctic Ocean transects. Upon statistical analysis, they conclude that sea ice draft changes geographically, but not temporally. This is perhaps due to the nature of sea ice during these transects, which occurred between 1960-1962. Further, LeSchack and Chang assume that the Central Limit Theory applies to the overall data set obtained by the submarine transits. In their view, the Root Mean Square (RMS) of the draft (Equation 10) is an appropriate indicator for roughness of a given area of sea ice.

$$RMS = \sqrt{\frac{1}{n}\sum_{1}^{n} d_n^2} \tag{10}$$

Where,

d_n = individual depth value recorded from the analog profile (m)

n = number of values used, between 3000 and 3500 data points for each calculation.

Cox and Schultz (1981) define sea ice roughness in terms of the height of the subsurface protrusions, which they call "features." These features create cavities, and those cavities are then classified as large or small, depending on the amount of oil a cavity might restrain from lateral spreading. The definition is heavily dependent on an equilibrium oil slick thickness, or the degree to which a slick will develop before gravity drives the slick to spread. The drawback to this definition is that equilibrium thickness is temperature dependent, and as oil viscosity is also temperature dependent, a "small" roughness for one type and viscosity of oil might be a "large" roughness for another type with a different viscosity.

Harder (1997) proposed an ice roughness coefficient, R, as the temporal integration of deformation work per area and time. As shown in Equation 11, sea ice roughness, R, is defined through local rates of change and advection balanced by environmentally induced stresses, strains, and melting.

$$\frac{\partial R}{\partial t} + \nabla \cdot (\vec{u}R) = \sigma \cdot \dot{\epsilon} + \frac{R}{h} \min\left(0, \frac{\partial h}{\partial t}\Big|_{thermo}\right) \tag{11}$$

Where,

R = roughness (J/m^2)

t = time (s)

u = horizontal ice velocity (m/s)

h = sea ice thickness (m)

σ = stress tensor (N/m^2)

$\dot{\epsilon}$ = strain rate (1/s)

Sea-ice dynamics cause changes in internal forces within a floe, resulting in deformation and leading to the quality of the ice being rough. Time, rather than thickness, then, is the driver of ice roughness. Further, R "represents the integrated history of the deformation of ice volume (Harder, 1997)."

From a momentum balance perspective, Steiner (1999) and Lu, P., et al, (2011) present sea-ice roughness as an element of the momentum exchange between the ice-ocean interface. Treatment of the topic primarily consists of determining a drag coefficient for ice floes in the context of atmospheric and oceanic modeling. Coefficients are often treated as scalar variables that are descriptive properties of the ice itself and may vary with ice conditions, but there is lack of agreement upon exact values that these variables should have at various conditions. Table 2 (Lu, P., et all., 2011). displays a summary of thirty-one separate coefficients to illustrate the challenge in developing a single, relatable number.

Table 2. Summary of ice-ocean drag coefficients, Cw.

Site	Ice Type	10^3 C_w	Level[a] (m)	Reference
Baltic Sea	moderately ridged ice	3.5	GSC	*Leppäranta* [1990]
Barrow Bay	1 km smooth floe	5.4	1	*Shirasawa and Ingram* [1997]
Barrow Strait	smooth landfast ice	1.32	1	*Langleben* [1982]
Beaufort Sea (AIDJEX)	1 km smooth floe	3.4		*McPhee and Smith* [1976]
Beaufort Sea (AIDJEX)		5.5	GSC	*McPhee* [1980]
Beaufort Sea (AIDJEX)		7.6	1	*Hunkins* [1972]
Beaufort Sea (AIDJEX)		2.0	GSC	*Hunkins* [1975b]
Beaufort Sea (AIDJEX)		4.1	1	*Langleben* [1980]
Beaufort Sea (AIDJEX)		5.0	GSC	*McPhee* [1982]
Beaufort Sea (AIDJEX)		20	1	*McPhee* [1979]
Beaufort Sea		3.4–3.8	2	*McPhee* [1989]
Beaufort Sea		5.5–6.2	5	*McPhee* [1989]
Bering Sea (BASICS)	rough floe	22.28	1	*Bruno* [1990]
Bering Sea (BASICS)	30 m rough floe	14.1	1.1	*Madsen and Bruno* [1987]
Bering Sea (MIZEX)	smooth floe	5.27	2	*Bruno* [1990]
Bering Sea (MIZEX)	rough floe	9.94	2	*Bruno* [1990]
Bering Sea (MIZEX)	smooth floe	5.94	2	*Madsen and Bruno* [1987]
Bering Sea (MIZEX)	100 m rough floe	17.6	2	*Madsen and Bruno* [1987]
Bering Sea (MIZEX)	smooth floe	7.8	2	*Reynolds et al.* [1985]
Bering Sea	rough floe	24.2	1.1	*Pease et al.* [1983]
Greenland Sea (MIZEX84)		7.1–8.3	1	*McPhee* [1989]
Greenland Sea (MIZEX84)		15.5–19.2	7	*McPhee* [1989]
Gulf of St. Lawrence	10 m rough floe	47	0.5	*Johannessen* [1970]
Gulf of St. Lawrence	rough floe	20–21	0.5	*Johannessen* [1970]
Hudson Bay	landfast ice	0.13–7.42	1	*Shirasawa et al.* [1989]
Lancaster Sound	landfast ice	7.3	1	*Shirasawa* [1986]
Robeson Channel	flat first-year ice	1.05	1	*Shirasawa and Langleben* [1976]
North Pole	3 km smooth floe	9	0.5	*Johannessen* [1970]
Weddell Sea		1.13	GSC	*Wamser and Martinson* [1993]
Weddell Sea	floes in polynya	3.05	GSC	*Kottmeier and Engelbart* [1992]
Weddell Sea		1.62	GSC	*Martinson and Wamser* [1990]

Numerous efforts have been made in literature to identify subsurface roughness from visible surface conditions. To this effort, Doble, Skourup, Wadhams & Geiger (2011) examined whether there is a relationship between ice draft (d) and the ice and snow surface elevation (f) over different ice types. Their definition of the relationship between d and f is given by Equation 12,

$$d = \frac{\rho_i f + h_s(\rho_s - \rho_i)}{\rho_w - \rho_i} \quad (12)$$

Where,

d = ice draft (cm)

f = snow and ice surface elevation (cm)

h_s = median snow thickness (cm)

ρ_s = snow density (kg·m^{-3})

ρ_i = isostatic ice density (kg·m^{-3}).

Taking the ratio of ice draft to surface elevation, the ratio $R = d/f$ showed a positive correlation when areal swaths for which R was calculated was less than eleven meters in diameter. Therefore, for small areas, there is some indication of subsurface roughness based on the relative deformation of the surface of the ice. The challenge with this finding in is the small areal footprint. Most satellites lack such tight resolution and achieving sufficient accuracy would require field measurements. It would appear that using surface roughness to gage subsurface roughness is only useful when scientists are in the field.

4.6 Draft Distributions

Research concerning the quantitative changes in Arctic sea ice have typically approached their investigations through the lens of mean sea ice thickness and concentration. More significant are the studies that research ice thickness distributions with their regional and seasonal variabilities, like those performed by Oikkonen and Haapala (2011). This work focused on changes in the pack ice from 1975-2000 as observed by submarines transecting the Arctic ocean. Instead of a single numerical value to describe ice draft for the entire Arctic ocean, Oikkonen and Haapala produced regional and seasonal histograms, showing a more cohesive picture of the ongoing changes.

Despite categorizing seasonal changes in terms of “Spring” and “Autumn,” which unfortunately lumps ice growing and thawing periods together haphazardly, the results are still quite telling. Regional draft changes indicate growth in the mean/modal draft in some areas, like

the Chukchi Sea, juxtaposed against an overall decrease, especially in regions such as the Beaufort Sea (Table 3, Oikkonen & Haapala, 2011).

Table 3. Regional spring and autumn mean and modal draft.

Region	Season	Mean/modal draft (m) 1975–1987	1988–2000	Change (m/decade)
1 North Pole	Spring	4.4/2.9	3.6/2.5	–0.6/–0.3
	Autumn	3.1/2.7	2.8/2.5	–0.2/–0.2
2 Canada Basin	Spring	4.2/2.5	3.4/2.3	–0.6/–0.2
	Autumn	3.1/2.1	2.4/2.3	–0.6/+0.2
3 Beaufort Sea	Spring	3.5/2.5	2.5/1.7	–0.8/–0.6
	Autumn	1.7/1.3	1.5/0.3	–0.2/–0.8
4 Chukchi Sea	Spring	3.1/2.5	2.4/1.5	–0.5/–0.8
	Autumn	1.2/0.1	1.4/0.3	+0.2/+0.2
5 Eastern Arctic	Spring	4.5/2.5	3.1/2.1	–1.1/–0.3
	Autumn	2.3/1.9	1.9/1.9	–0.3/0
6 Nansen Basin	Spring	3.3/0.1	3.4/2.1	+0.1/+1.5
	Autumn	2.7/1.9	2.8/1.9	+0.0/0

The histograms of the binned data show a trend from, “one high peak to a clearly bi-modal structure (Oikkonen & Haapala, 2011).” That bi-modal structure is indicative of the overall transition from dominant multi-year ice to first year ice within each area of study (Figure 4, Oikkonen & Haapala, 2011). Lastly, the data distribution follows a characteristic shape of a negative exponential distribution, though nowhere in the discussion was this mentioned.

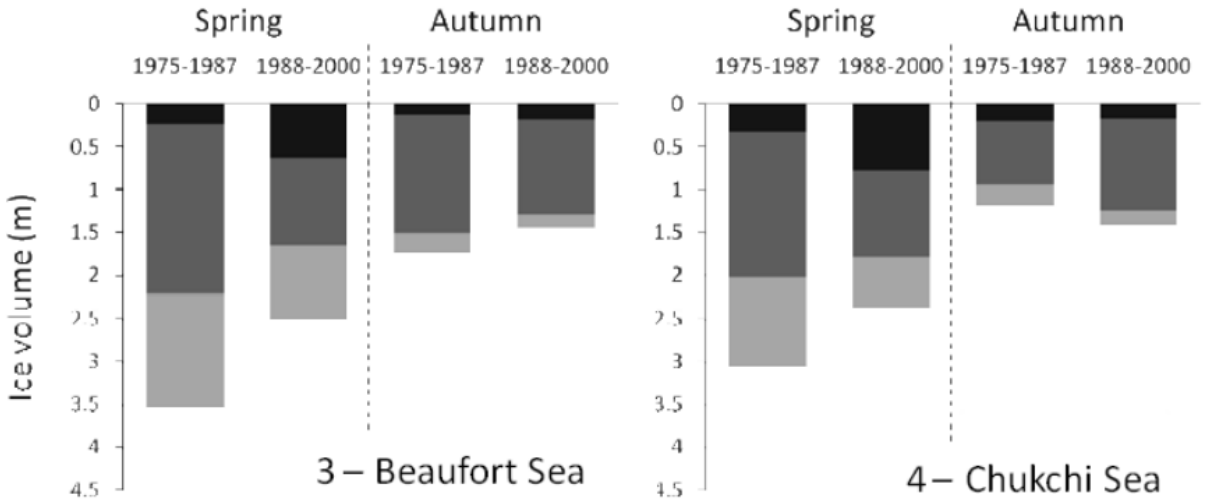

Figure 4. Regional mean sea ice draft and composition for Beaufort and Chukchi Seas.

Regional mean sea ice draft and composition for Beaufort and Chukchi Seas. Looking at ice draft from the perspective of applied loads, Wadhams and Toberg (2012) investigated the shape and form of ice keels. Ice keels are classically defined as ice that is deeper than an assumed threshold value, h_{thres} (Figure 5, Wadhams & Toberg, 2012). The motivation for the study was to validate whether numerical models for ice loads, which assume a triangular draft, were correct. Using draft data from Fram Strait, Wadhams and Toberg (2012) found that ice keels roughly follow a negative exponential distribution and are most frequently trapezoidal in shape (Figure 6, Wadhams & Toberg, 2012). An example of an ice ridge cross section

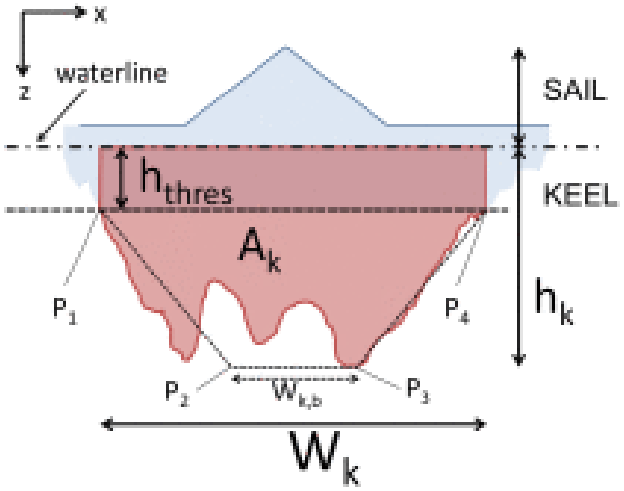

Figure 5. An example of an ice ridge cross section.

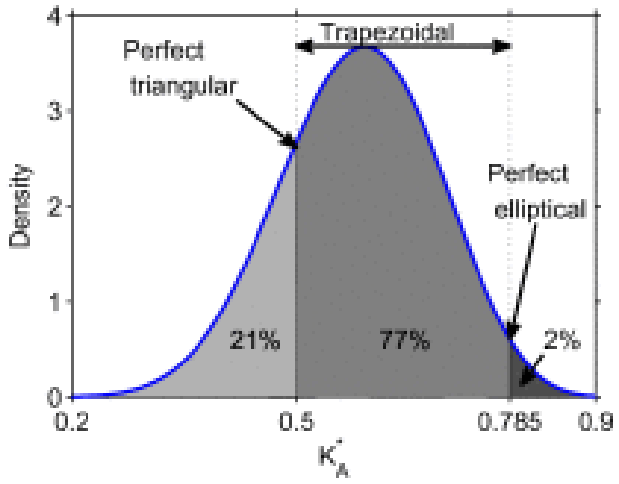

Figure 6. Probability density of mean keel area coefficient.

Probability density of mean keel area coefficient Investigating sea ice thickness, Fukamachi et al. (2017) measured sea ice draft and velocity near Point Barrow, Alaska. Using an ice profiling sonar and an acoustic doppler current profiler moored to the sea floor, they obtained information during the 2009-2010 winter about ice passing over the equipment. While the team was focused on determining sea ice thickness from their measurements, their publication utilized an ice-draft statistical analysis. The analysis shows that the ice drafts are characterized by bimodal data set, with peaks at drafts < 0.2 m and between 1.2 and 1.4 m (Figure 7, Fukamachi et al., 2017). Further, the data qualitatively follows a negative exponential distribution in the range of 3-15 m, similar in shape to observations by Wadhams, Hughes and Rodrigues (2011),

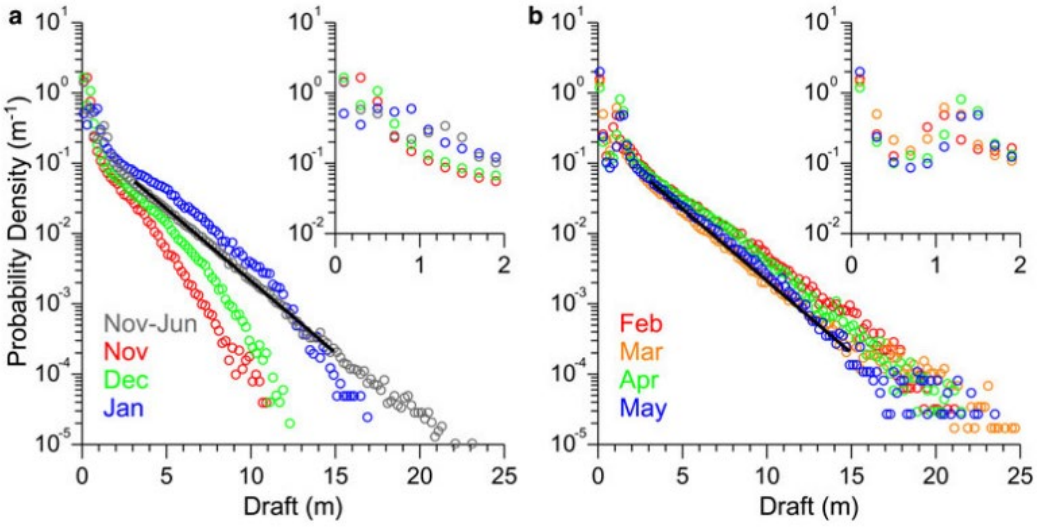

Figure 7. Semi-log scale of sea-ice draft probability density function.

and Wadhams and Toberg (2012) in their respective studies. . Semi-log scale of sea-ice draft probability-density function.

Regional currents and bathymetric characteristics play an important role in the development of sea ice subsurface shapes. As seen in the Oikkonen and Haapala (2011) work, the eastern Arctic tends to have deeper autumnal drafts, and shallower spring drafts. The Arctic region focused on in this thesis is to the west, off the coast of Alaska, where drafts tend to be slightly shallower. It is curious, though, that despite regional differences in draft depth, draft distributions are strikingly similar in their form. As seen in these papers, and others, (Gaver and Jacobs, 1982; Valenti, 2015), an exponential distribution, a special case of the Weibull distribution, is a likely candidate for best fit for this natural phenomenon.

4.7 Subsurface Volume

Oil spill models require comprehensive environmental inputs in order to determine the fate and transport of the oil. While effort has been made to determine oil slick fate in water where ice is present, current models are inadequate when oil is trapped beneath the ice. Critical research on the complexity of different ice regimes has yet to be performed. This dearth of research leaves models without a method for accounting for the influence of the subsurface on the motion of the oil particles (Fingas & Hollebone, 2003; Wilkinson, Wadhams & Hughes, 2007). The lack of a comprehensive picture of under-ice topography is concerning from the lens of natural resource development as efforts like oil drilling and exploration pose significant hazards to local ecosystems. To ensure safe development, efforts must be made to better define this unique subsurface.

Emerging methodology for mapping the bottom of sea ice includes the use of underwater autonomous vehicles (UAVs). UAVs have the ability to create 3-D images of the interface between the ice and water. By viewing the topography of the underside of the ice, researchers can determine both the volume of the space created by the ice and estimate the direction an oil slick would take (Wilkinson, Wadhams & Hughes, 2007). This critical work addresses two important issues. First, past Arctic sea ice research assumes a lack of spatial variability in under-ice topography. This assumption is underscored by the use of a single empirical parameter to

describe ice roughness in current models. Second, modelers have not considered how subsurface roughness of different ice regimes impact oil spreading.

In field work from 1977 to 1980, it was determined that fast ice has a range of storage capacity from 10,000 to 60,000 m^3/km^2, or 1 to 6 cm of average pooling depth, with a mean pooling capacity of 33,860 m^3/km^2 (3.34 cm) (Table 4, Wilkinson, J., Wadhams, P., & Hughes, N., 2007). Wilkinson, Wadhams, & Hughes (2007) validated this work with field work in Greenland also using fast ice. In their work, Wilkinson, Wadhams and Hughes modeled the subsurface of fast ice, or ice that is attached to shore. Volume beneath the ice was calculated using Equation 1, the definition of sub-surface storage capacity by LeShack and Chang (1977). The characteristic roughness of the fast ice was noted in terms of the standard deviation of the ice draft from the mean. For Wilkinson, Wadhams, & Hughes, the ice in their study had a mean draft of 1.26 m, and a standard deviation of 0.1 m.

Table 4. Summary of potential pooling volume for oil released beneath fast ice.

Site	Date	Mean ice draft (m)	Std dev. ice draft (m)	Oil pooling capacity (m^3/km^2)	Reference
Prudhoe Bay	1977	1.90*	N/A	27,500	Kovacs 1977
Tigvariak Island	1978	1.55*	0.03	32,000	Kovacs et al., 1981
Reindeer Island	1978	1.33*	0.01	10,000 (Min)	Kovacs et al., 1981
West Dock site	1979	1.83*	0.15	60,500 (Max)	Kovacs et al., 1981
Site A	1980	1.52*	N/A	24,800	Kovacs et al., 1981
Site B	1980	1.59*	N/A	23,900	Kovacs et al., 1981
Site C	1980	1.59*	N/A	51,300	Kovacs et al., 1981
Prudhoe Bay	1978	1.24	N/A	47,000	Barnes et al., 1979
Stefansson Sound	1978	1.50	N/A	25,400	Barnes et al., 1979
Tidal inlet	1978	1.40	N/A	36,200	Barnes et al., 1979
Mean of above surveys		1.55**	0.20	33,860	
NE Greenland	2004	1.26	0.10	30,102 (Max: 72,165 Min: 19,731)	This paper

The researchers discovered that current assumptions about the storage volume beneath fast ice varies significantly even though the subsurface elevation in their study did not. Further, they illustrated that the heterogeneous nature of the subsurface cannot be quantified by a simple

parameter. Instead, the authors proposed a range of volume storage space is the better descriptor of the true nature of the ice. Using a range of storage values supports the prior work that inspired this thesis.

5 Methodology

5.1 Draft Data

Input measurements for ice draft came from the North Slope Science Initiative (NSSI) who obtained the information from Shell Exploration and Production Company (Shell). Shell contracted with ASL Environmental Sciences Inc. (ASL) to collect the subsurface ice draft data in the Beaufort and Chukchi Seas. Data collection began in the Beaufort Sea in 2005, expanding to the Chukchi Sea in 2008 (Figure 8, BOEM, 2015). In the Beaufort, five different locations

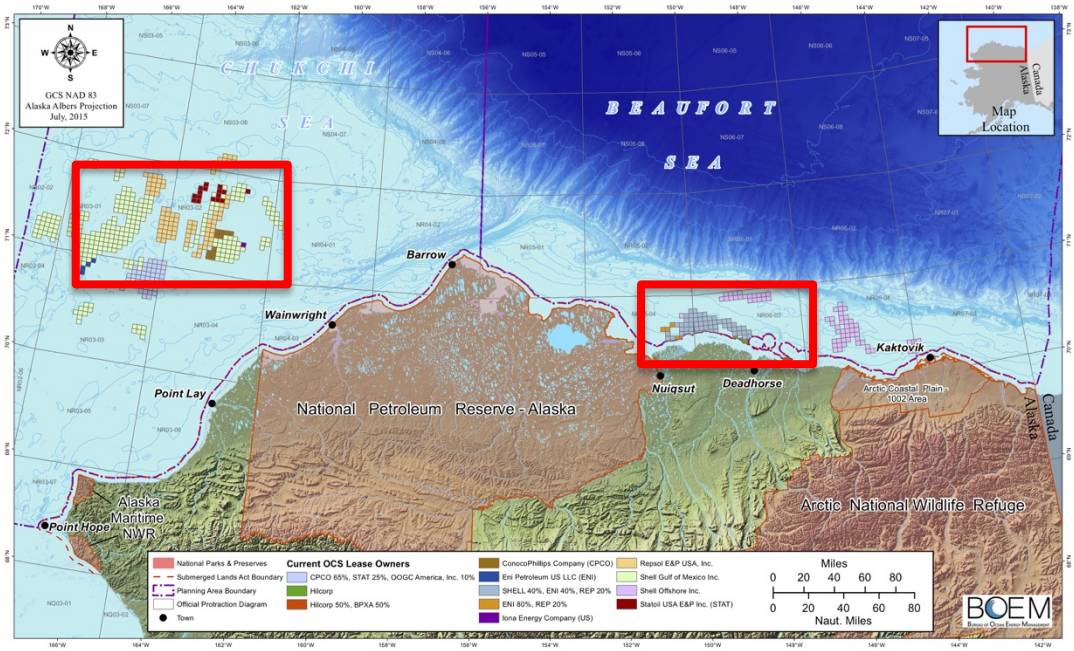

Figure 8. General locations (in red) of Shell data collection sites.

were used over a period of five years. In the Chukchi, measurements varied among four locations over an eight-year time frame. For these programs, two tandem sensors were deployed consisting of an ASL Ice Profiling Sonar (IPS-5), manufactured by ASL, and the Teledyne RD Instruments Acoustic Doppler Current Profiler (ADCP) (Figure 9, Mudge et al., 2014). These instruments made direct measurements of ice draft (m), ice velocity (m/s), and ocean current profiles. The time resolution on the draft measurement was once every one-to-two seconds, with a horizontal

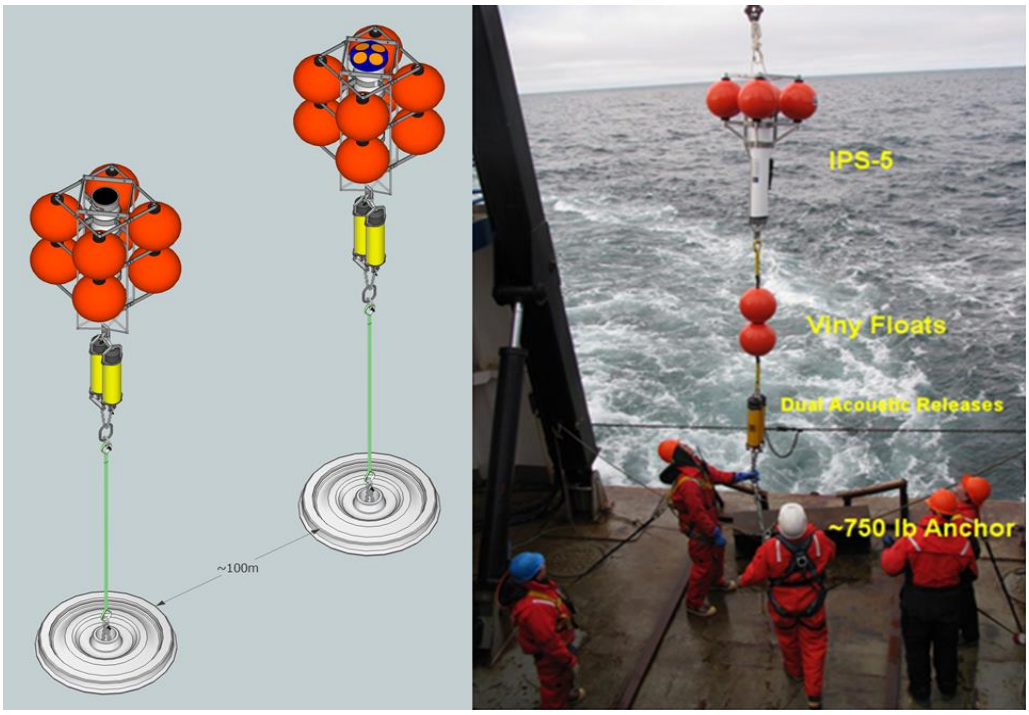

Figure 9. Schematic of the moorings for IPS (left) and ADCP (right).

resolution of 1.0 m, and a vertical resolution of 0.025 m. Ice velocity and ocean current profiles from the ADCP were recorded with a time resolution of once every fifteen minutes in 2008-2009 and reduced to once every five minutes from 2009 to 2014.

Profiler pairs were moored in water between 20.0 and 40.0 m deep and took continuous recordings for up to a year at a time. Each instrument set was recovered annually to replace batteries, perform regional calibrations, and allow download of the data. Timing checks were performed on the instrumentation to measure clock drift. Once checks were complete, the profilers were immediately redeployed to their same mooring site.

This project used data sets collected between 2010 and 2013 in the Beaufort (at 'Site A') and in the Chukchi Sea (at site 'Crackerjack').

5.2 Surface Conditions

The ice stage above each ADCP/IPS data point during the 2010-2013 measurement period was obtained from AOOS (Appendix A and B). Ice stage data is available in the form of the ice egg code (Figure 1) and is available on a weekly basis. The available code includes

fourteen ice stage designations. This project converted ice stage at a given location and time into a single, comma separated identifier, such as ‘1,3,7’ or ’10,11,12’. This project is specifically concerned with an ice stage reported as ‘7,10,12,’ which has a primary condition of first year ice.

Draft data was then imported into MATLAB. Since the surface conditions are not provided on an hourly, or even daily, time frame, the assumption was made that surface conditions are consistent for seven days (Sunday to Saturday). In reality, this assumption seems illogical, but more accurate surface data is unavailable. Therefore, for each week there was a reported surface ice condition of ‘7,10,12,’ draft data for that weekly period was extracted, and compiled in another array (Appendix C). There are approximately nine hundred thousand data points for the three time periods, but a full listing of those measurements is not included in the Appendices for brevity.

5.3 MATLAB Analysis

The raw ice draft data were processed by ASL who followed established procedures documented by Melling et al. (1995), Fissel et al. (2008) and ASL Environmental Sciences Inc. (2011). This procedure converted the time-of-travel recorded data into a spatial data series using the recorded ice velocities. The processed data is provided in *.dat* files and each file has a time header showing the date when measurements began. This date is in standard year/month/day/hour/min/second format, but draft data is provided with a Unix time stamp. For convenience, all headers were converted to Unix time codes.

There were four timeframes in which the observable conditions met the ‘7,10,12’ specification. These timeframes were the weeks of January 24-30, 2011; April 4, 2011 to June 5, 2011; May 16 2013 to June 19, 2013; and July 9-15, 2014. These time frames were converted to Unix time in MATLAB, and data measured within these weekly periods were extracted for analysis. It should be noted that draft measurements were not available for the week of July 9-15, 2014. It appears the batteries in the IPS failed prior to this period leaving no draft data available.

5.4 Statistical Analysis

The purpose of this statistical analysis is to determine which distribution best fits the measured ice draft data. Fitting the data to a distribution allows for the prediction of the frequency of draft depths with probability density functions. If the subsurface draft conditions are predictable, then oil spill modelers can reliably forecast where oil will pool beneath the surface of sea ice in a live spill incident. The consensus in the literature review indicates that sea ice draft data follows a negative exponential distribution.

5.4.1. Histogram

To qualitatively identify potential distributions to fit the draft data, histograms of the draft data were produced (Figures 10 and 11).

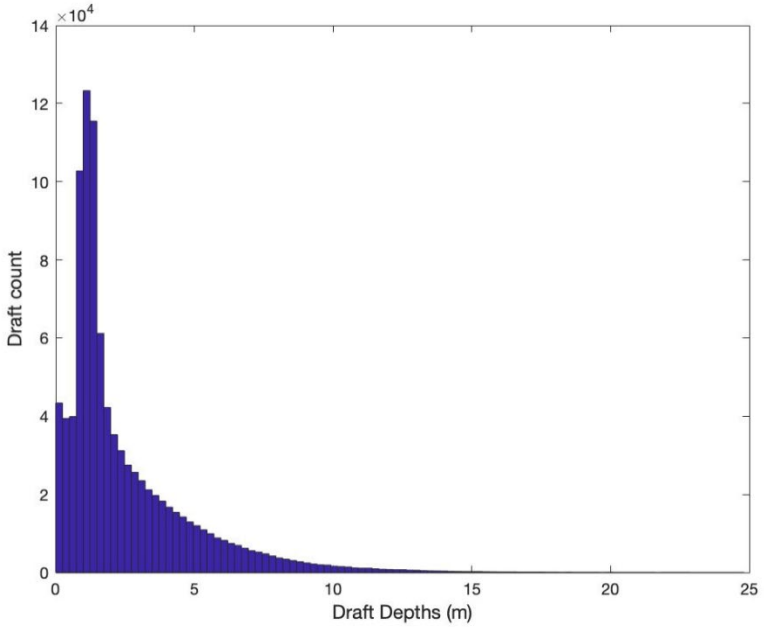

Figure 10. Ice condition '7,10,12' histogram with 100 bins.

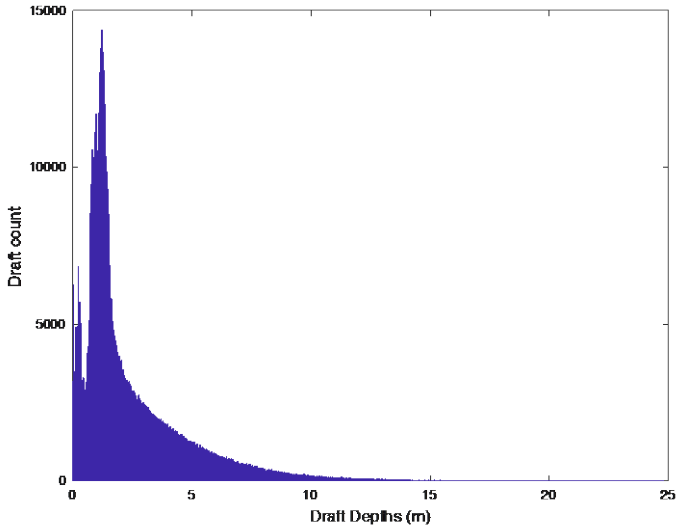

Figure 11. Ice condition '7,10,12' histogram with 1000 bins.

Histograms approximate the probability density function for large sample sizes. For each rectangular interval, or 'bin,' the area of the bin represents the relative frequency of the measurements in the interval. That frequency provides an estimate of the probability that a given draft measurement (d) falls in the interval [d_{min}, d_{max}].

These histograms were divided into 100, and then 1000 bins, respectively. Lower bin sizing appeared to be too rough, and detail about the data was lost. Analysis continued with n = 1000. Draft measurements are continuous within the domain. The figures indicate a right skewness to the data, alternatively described as being positively skewed. From these characteristics, potential distribution candidates are: Log-Normal, Exponential and Weibull.

In Figure 10, and slightly more evident in Figure 11, the data also appears to be bimodal; there seem to be two peaks in the histogram. Exploring the apparent bimodality of the data, the data was separated so that a more detailed inspection could occur. First, the bin with the peak number of draft measurements was identified. The bin with the largest number of data points has edges of 1.2-1.3 m. Then, to find the inflection point for the first curve, draft data was separated into two sets: drafts below 1.3 m, and drafts above 1.3 m.

The local minimum in the shallow draft set was determined to fall in the bin with edges between 0.48 m and 0.50 m. The total draft data was then separated again into three new sets:

drafts below 0.49 m, drafts between 0.49 and 1.4 m, and drafts above 1.4 m (Figures 12, 13, and 14). The size of the bins was kept at 0.1 m for all figures for consistency.

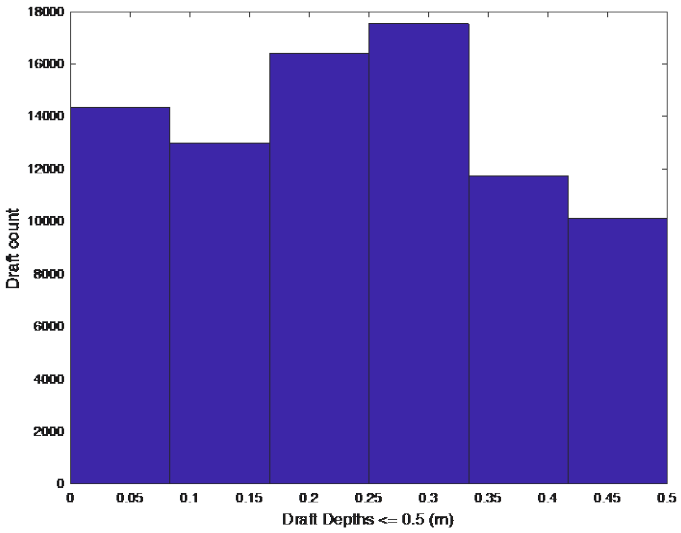

Figure 12. Draft measurements less than 0.5 m.

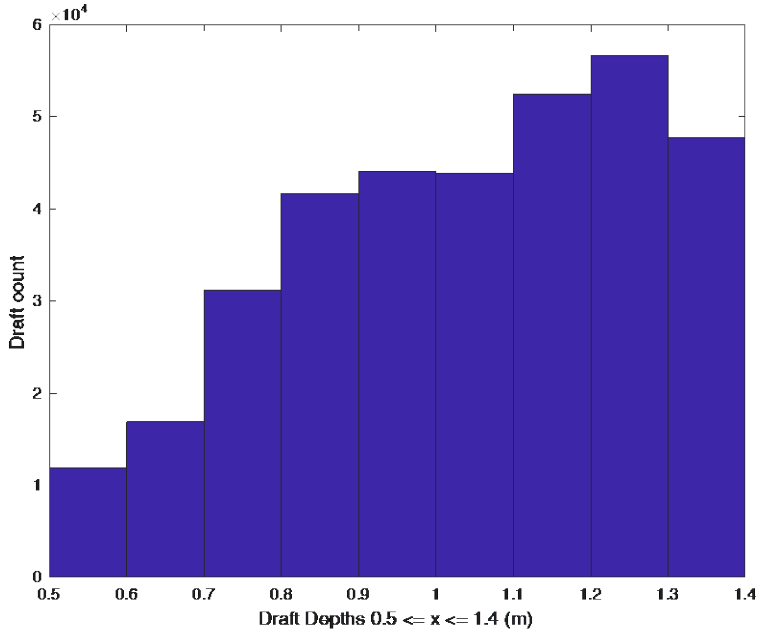

Figure 13. Draft measurements between 0.5 and 1.4 m.

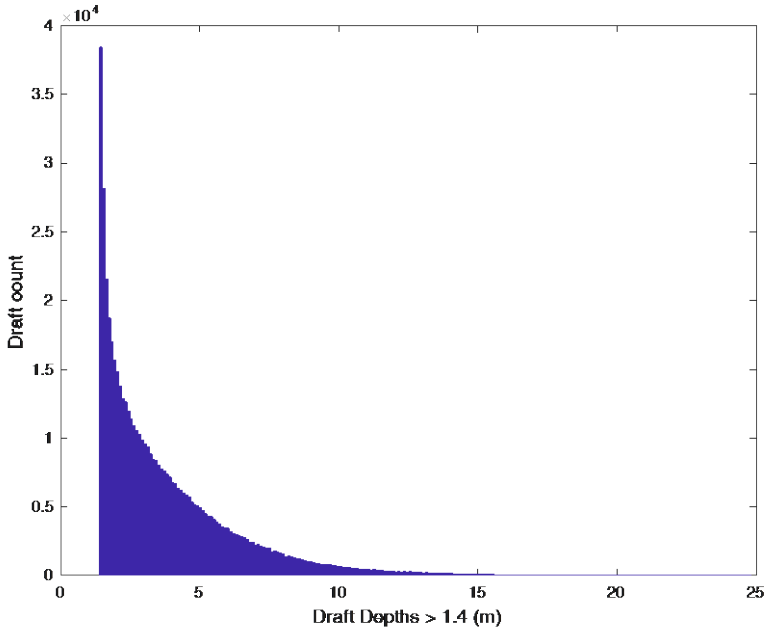

Figure 14. Draft measurements greater than 1.4 m.

5.4.2 Central Tendency

The calculated geometric mean for the data set is 1.65 m, and the arithmetic mean of the data was calculated at 2.51 m. The mode of the data was between 1.2 m and 1.3 m, with a standard deviation of 2.41 m. The arithmetic mean in Figure 15 appears weighted toward the right of the graph. With a dominant draft depth between 1.2-1.3 m, the arithmetic mean of 2.51 m appears to be an inappropriate measure of the central tendency of the data.

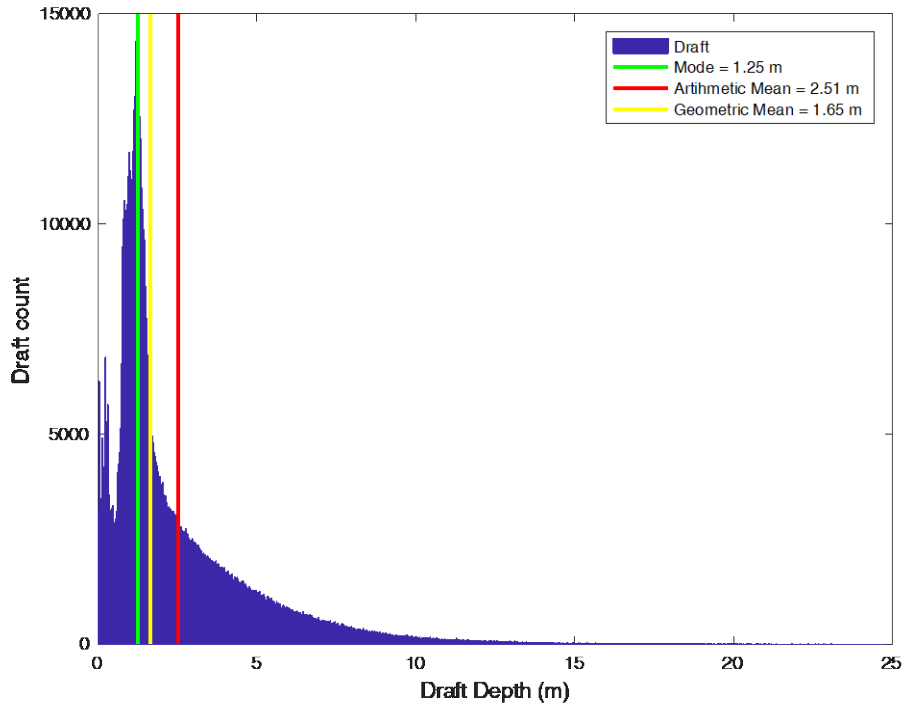

Figure 15. Comparison of the mode, arithmetic, and geometric means.

Arithmetic means are subject to skewness when outliers are present and are more appropriately used for normally distributed data. When calculated, the arithmetic mean indicates the average draft per measurement. When a data set is comprised of information that is not independent and has large fluctuations in size or scale, calculating a geometric mean is more descriptive of the central tendency of the set. Regarding ice drafts, draft measurements are not completely independent of the measurement just prior and just after a given value. There are also large outliers present in the overall set, which is apparent from the histogram in Figure 15.

To account for the influence of the draft outliers and interdependence, the geometric mean was calculated. Geometric means 'normalize' the range of data being analyzed, such that no one range dominates the outcome. Using Equation 13 (Weisstein, 2019), the process takes the n^{th} root of the product of the individual draft measurements, where n is the number of recorded draft entries. As seen in Figure 15, the geometric mean is a better measure of the central tendency of the draft data.

$$\left(\prod_{i=1}^{n} x_i\right)^{1/n} = \sqrt[n]{x_1 x_2 \dots x_n} \tag{13}$$

5.4.3. Distribution Fitting

The draft measurements used in this thesis are continuous and are observed to be asymmetric. From this observation, then, five potential distributions are candidates for fitting the data. These are the Exponential, Lognormal, Gamma, Weibull, and Minimum Extreme Value distributions. Narrowing the selection further, it is noted that the outliers are positive, removing the Minimum Extreme Value distribution from the list.

Having narrowed the potential distribution choices down to Exponential, Gamma, Log-normal, and Weibull, analysis continued to verify the assumption that one of these four choices was correct. This method employs a subjective visual examination of the data to test how well the data conforms to a hypothesized distribution. First, each of the four distribution curves were projected onto the histogram of draft data. Each curve is calculated based off of the mean, variance and shape factors specific to the distribution, as determined from the data set. As seen in Figure 16, it is clear that neither the Lognormal nor the Weibull distribution are a good candidate to fit the data. This leaves Exponential and Gamma distributions.

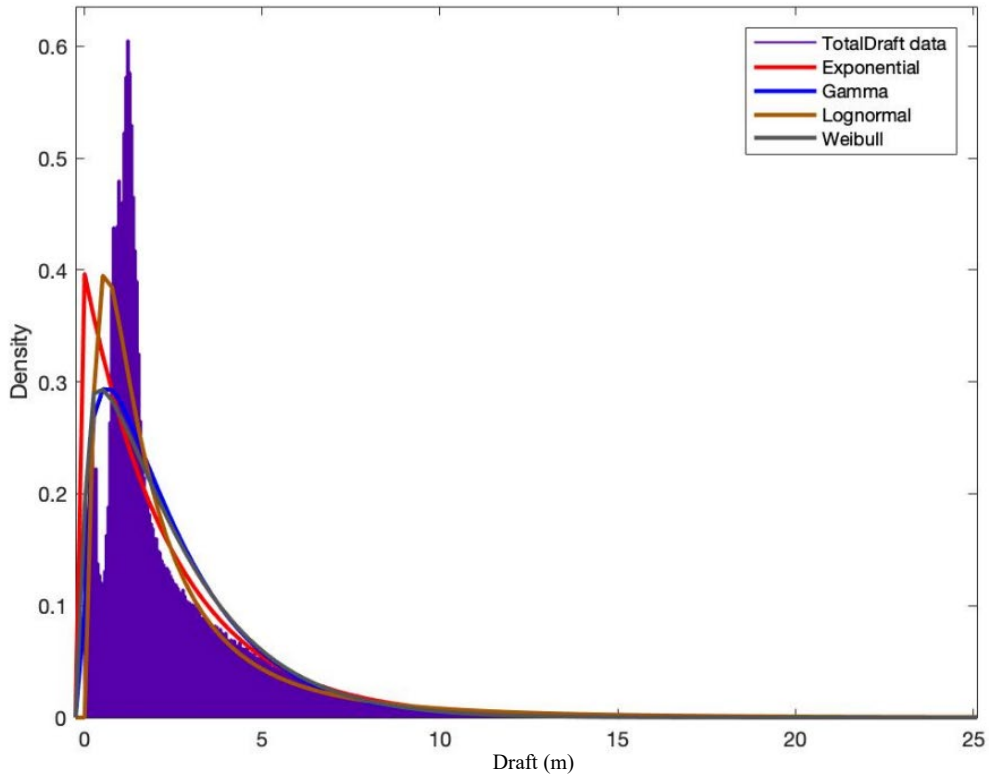

Figure 16. Distribution fitting for draft data.

The next step was to plot the draft data against the observed cumulative frequency of those observations. If a hypothesized distribution is correct, the data points should fall along the idealized line for the distribution. Figure 17 illustrates that the exponential and gamma curves are indeed a better fit. As the Exponential distribution is more closely aligned with the observed data, it seems to be the natural choice for best fit, with the Gamma distribution a close runner up. The positive skewness to the data is illustrated toward the right-hand side of the figure; the data points there do not align with the distribution.

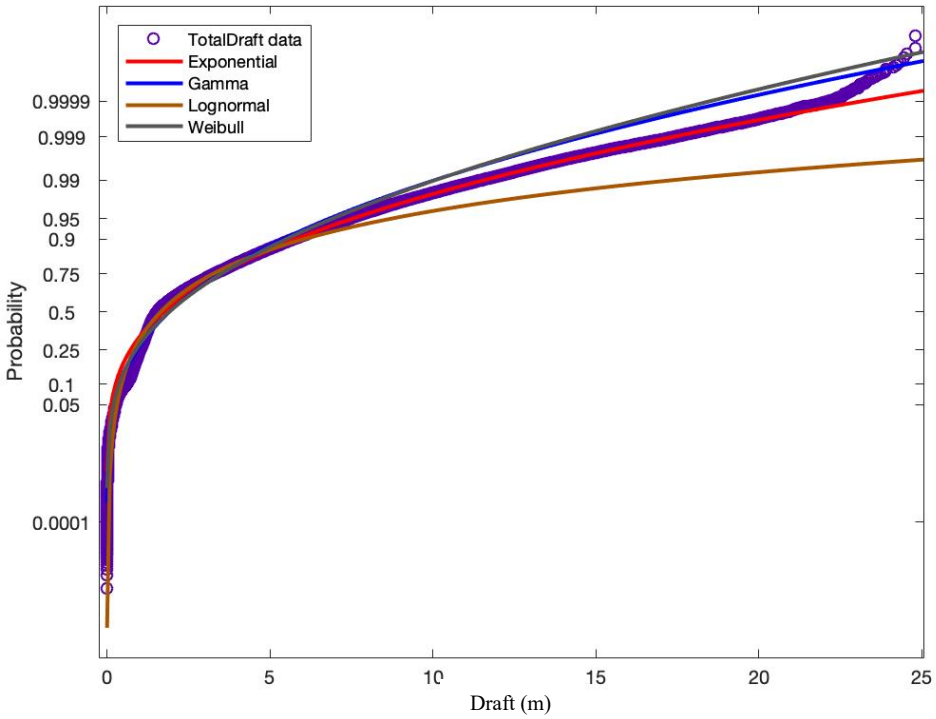

Figure 17. Probability plot for data compared to various distributions.

Looking at the exponential distribution more closely, the Cumulative Distribution Frequency (CDF) plot was employed. The formula for the exponential CDF is given by Equation 14 (Montgomery & Runger, 2014),

$$F(x) = P\{X \leq x\} = 1 - e^{\frac{(-x)}{\mu}} \tag{14}$$

where μ is the arithmetic mean of the data, and x is an observed draft depth (m). Equation 14 can be transformed into a linear relationship (Equation 15) between $F(x)$ and x by,

$$-log(F(x) - 1) * \mu = x \tag{15}$$

Graphing x, the measured draft depth, and y = $-log(F(x) - 1) * \mu$, it is observed in Figure 18 that the exponential distribution is an excellent fit for the data, even with the influence of the skewed data tail. Code for the statistical analyses can be found in Appendix D.

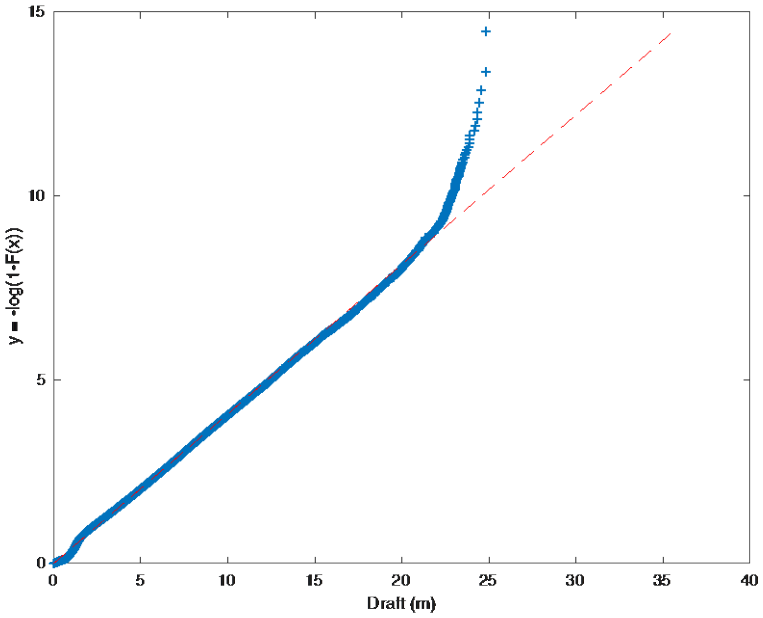

Figure 18. Linearized exponential CDF plot.

5.5 Goodness-of-Fit

To test the appropriateness of the exponential distribution, a test was performed using the chi-square test. Since the underlying distribution for the draft data is unknown, it is important to test the hypothesis that any proposed distribution will be an appropriate fit for the data. A sample of n = 500 random data points was extracted from the total draft measurements. Those n observations were sorted least to greatest, and the test statistic χ^2 was computed with Equation 16 (Montgomery & Runger, 2014).

$$\chi^2 = \sum_{i=1}^{n} \frac{(O_i - E_i)^2}{E_i} \tag{16}$$

In Equation 16, O_i are the observed counts of draft data, and E_i are the expected counts based on the hypothesized distribution. The Chi-square test was performed for all three distributions to check the validity of the assumption of an exponential distribution as best fit. Those test statistics are summarized in Table 5.

Table 5. Test statistics from the Chi-square test.

	h_0	h_1	p-value	X^2	degrees of freedom
Exponential	1	0	0.5731	3.8369	5
Gamma	0	1	5.927×10^{-7}	31.7435	3
Lognormal	0	1	0.0105	14.9711	5
Weibull	0	1	0.0014	17.6724	4

In Table 5, h_0 is the null hypothesis that the data does not come from the proposed distribution. If the returned value is '0', then the test failed to prove that the data came from that distribution. If h_0 equaled '1', then the null hypothesis failed, and the alternative hypothesis (h_1) that the data does fit the prescribed distribution, is true. The test is performed for alpha = 0.05. The chi-square test statistic threshold values can be found in table form, organized by alpha and degrees of freedom. For three degrees of freedom, the test statistic threshold value is 7.82; four degrees of freedom, the test statistic threshold value is 9.49; for five degrees of freedom that value is 11.07 (Mongomery and Runger, 2014). Therefore, all except the exponential distribution failed to reject the null hypothesis. The best distribution to fit the observed draft data is an exponential distribution.

5.6 Data Generation

Having justified fitting an exponential distribution to the ice draft data in 2-D (distance x, draft depth z), the assumption is made that the distribution holds regardless of the directionality taken to obtain the draft measurements. Along any given transect, the distribution of data along a 1 km segment should follow an exponential distribution. Given the multiple observations in the literature review indicating consensus over the exponential distribution, all from dissimilar

transect paths and data collection locations, this appears to be a reliable assumption. If true, then a stochastic model can be constructed from an array of randomly generated ice draft data following an exponential distribution in three dimensions.

To develop such an array, random draft measurements were constructed on a grid measuring 1000 m (1 km) by 1000 m (1 km), with draft depths simulated every 1 m. Draft depths were produced with a random number generator in MATLAB, following an exponential distribution. The arithmetic mean of the actual ice draft data was used as the mean ($\mu = 2.51\ m$) for the randomly generated data. The output was then translated to a comma separated file (.csv) for upload to ArcGIS and further analysis. Code for the simulated draft array is found in Appendix E. Processing time for the array took eight hours.

5.7 ArcGIS Modeling

The modeled draft data was imported into Arc Map from the MATLAB generated csv file. That file was then converted to a vector storage data format, or shape file, which allowed for geographic attributes to be analyzed more carefully. Each data point, or node, represented a unique *x* and *y* location, and a draft height, *z*. Those nodes were then connected through triangulation networks, forming the frame of the surface to be modeled. Each edge within the network formed adjacent, non-overlapping triangular facets.

With the framework in place, the image was then rasterized using natural neighbor interpolation. This process built the surface over a triangulated network. Natural neighbor interpolation takes a query node and identifies the closest neighboring nodes. Each neighboring node given a weight, or influence value, based on proportionate areas. That weight determines the slope of the surface between the nodes. The result of this process is a smooth surface, with the caveat that the function cannot infer trends between nodes that are not part of the data set. Figure 19 illustrates the contour plot over the rasterized image on the left, and then the contour

plot alone on the right. On the edges of the contour, the elevations, in whole numbers are marked.

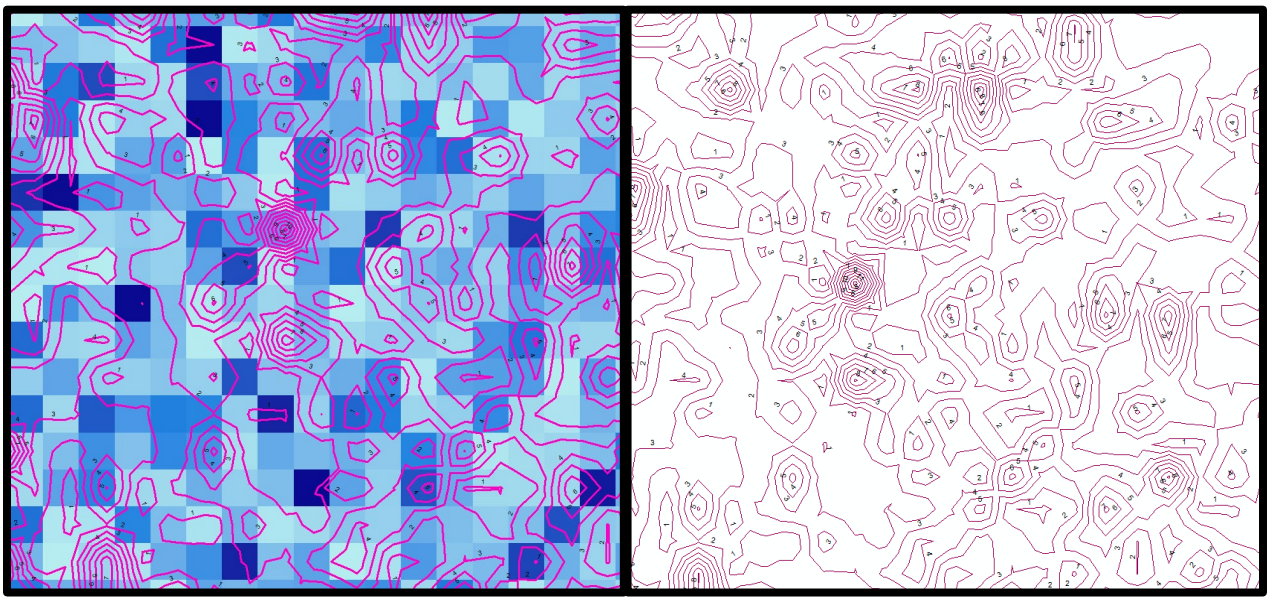

Figure 19. Raster image with contour overlay for surface ice condition

Once the rasterized surface was rendered, volume calculations were performed. This required the overlay of a horizontal plane parallel to the x-y plane of the draft surface. This plane was offset a distance of $z = 2.51$ m, the arithmetic mean of the original data, and is pictured in Figure 20 in black. The 'void' space, or the assumed maximum volume of potentially stored oil is the volume between the surface of the ice and the mean draft plane.

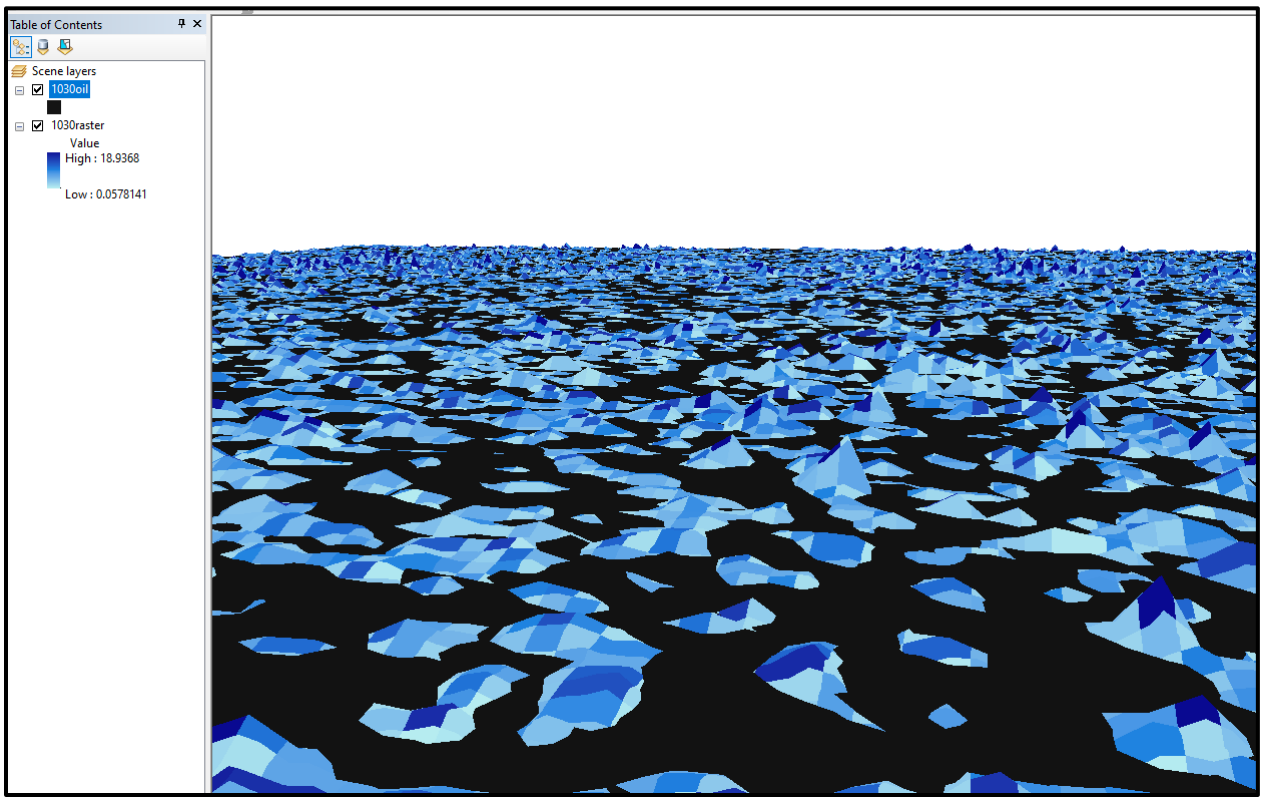

Figure 20. The subsurface of the sea ice is modeled in ArcGIS, upside down, for illustration.

The total volume between the ice surface and the mean draft, over a 1 km square area, is 415,991 m^3/m^2. Supporting values for this storage calculation are found in Appendix F.

6 Discussion

The result of the volume calculation was surprising. Recall from Figure 3, that for an observed ice condition of '7,10,12, the previously proposed volume ranged between 15,000 m^3/km^2 and 50,000 m^3/km^2. Obtaining a result of 415,991 m^3/m^2 is incongruous with the original study. This disagreement in results leads to two questions: which capacity calculation is correct and why don't they agree?

Literature that is available is mostly focused on fast ice, or ice attached to shore. Fast ice experiences bottom smoothing due to its stationary behavior and the current flowing over the underside. Recall that Yapa and Chowdhury (1990) determined experimentally that 0.1-2 cm was the maximum depth of an oil slick, under fast ice, before external driving forces overcome surface tension. For completely smooth ice, this depth can be multiplied into an overall storage capacity of 20,000 m^3/km^2.

For an observed surface condition of '7,10,12,' the original 2-D study proposed a range of 15,000 m^3/km^2 and 50,000 m^3/km^2 of storage capacity. This equates to a range of 0.015 m (1.5 cm) to 0.050 m (5.0 cm) over a square kilometer of older, first year ice. It seems incongruous that having gone from very smooth to very rough ice, the storage capacity would only increase from 2 cm to 5 cm in average thickness. While the results from the 2-D study are satisfactory for preliminary efforts, it is far more logical that older, first year ice could store more oil in the cavities between drafts.

Draft to draft, the depth of the ice between data points doesn't reduce down to a zero depth; instead it would likely be high enough to enclose more oil than the previously suggested 5 cm. Literature also indicates that keels form more trapezoidal shapes than triangular ones, which may account for some error in volume calculations. Modeling that shape requires a more sophisticated software in which the nearest neighbor algorithm for the surface mesh can be adjusted locally around the peak draft measurements.

In the ArcGIS model, the output of 415,991 m^3/km^2 equates to an average static depth of 0.42 m (42 cm). Looking at this another way, it was determined that 92.3% of the total draft measurements exceed the 42 cm depth. At 42 cm, the oil slick would cover just 7.6% of the total drafts in that area. For the observed surface condition of '7,10,12,' and in the absence of thermal and hydrodynamic influences, this is a more reasonable maximum depth for an accumulated oil.

Due to time constraints, it was not feasible to reanalyze all of the original data from the initial study. That analysis had been performed in conjunction with another project and new algorithms would need to be written. However, the process of linearly extrapolating a 2-D draft set into 3-D, then computing the volume, could be examined. Another array of randomly generated data was created, following an exponential distribution and using the same arithmetic mean. When extrapolated, the shape of the 3-D domain took the form seen in Figure 21.

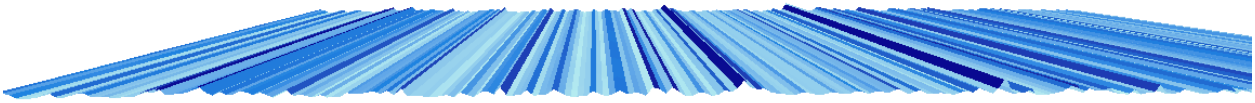

Figure 21. 2-D draft heights linearly extrapolated over a 3-D domain.

When volume was calculated for this domain, from a draft mean of 2.51 m down to the surface, the result was a volume of 52,675 m^3/m^2, or an average depth of 5.27 cm. This result answered two things. First, it shows that the linear extrapolation method does overestimate the amount of sea ice present in a given area. That overestimation severely depresses the storage capacity beneath the surface, which would affect efforts to properly model oil slick spreading. Second, it shows that the original study was not erroneous, and that the currently accepted methodology for computing storage capacity was correctly applied.

It is unclear whether the currently accepted definition of storage capacity from LeShack and Chang (1977) has been tested prior to this thesis work. Without advanced modeling software, it would have been difficult to properly assess the complex three-dimensional structures of sea ice, and impossible to ascertain whether the volume capacity was being over or under estimated by the process. In the course of this work, though, no literature could be identified which challenged either the assumption that draft distributions follow a normal distribution nor that a 2-D area calculation multiplied by the length of the domain was a proper method. If the results in this current work can be verified through further analysis, it calls into question the inherent assumptions oil spill models currently utilize. If ice is being over estimated, then an Arctic oil spill slick could move much more quickly beneath the ice than currently

predicted. The impact of such an erroneous assumption would lead to increased environmental threats to humans and wildlife in coastal regions.

Having identified why the 2-D and 3-D models disagreed, how then does the 3-D model fit the relevant literature? Returning to the work of Fukamachi et al. (2017), the analysis of this particular subset of the total draft data does follow what the other researchers found. Namely, that there's a bimodality to the draft data, with an overall mode between 1.2 and 1.4 m. The shape of the data, with its characteristic negative exponential curve, also matches those findings by Wadhams, Hughes and Rodrigues (2011), and Wadhams and Toberg (2012). As the data fits within the general scheme of what other researchers discovered, it follows that the modeled data is also a proper representation for actual sea ice with this observed surface condition.

Further effort must be made to determine an appropriate methodology for calculating subsurface storage capacity. If the approach taken by LeShack and Chang is found to be invalid for a three-dimensional domain, then further efforts are required to provide the scientific community with a new way to calculate storage capacity. There is also little in the way of a proper, experimentally supported, definition of "roughness." When it was thought that ice drafts followed a normal distribution, standard deviation was a good relative measure of roughness. The greater the deviation, the rougher the ice. However, as illustrated in this work, ice drafts are not normal, and therefore a different measure of the subsurface variability must be employed.

One of the other considerations that neither the 2-D or the 3-D model can account for is the influence of pressure ridges. Pressure ridges present unique subsurface barriers to oil slick motion. Similar to massive walls of ice, they would inhibit motion of trapped oil, slowing the slick motion, and might influence localized pooling. Pressure ridges would also account for a larger volume of ice in a given region, changing the relative storage capacity. If there were ridges on the floes that passed over the ULS sensors, they would not have been recognized as such. Future efforts to better model the subsurface of sea ice will need three-dimensional data, like that pictured in Figure 22 (Wadhams, 2012), from side-scan sonar.

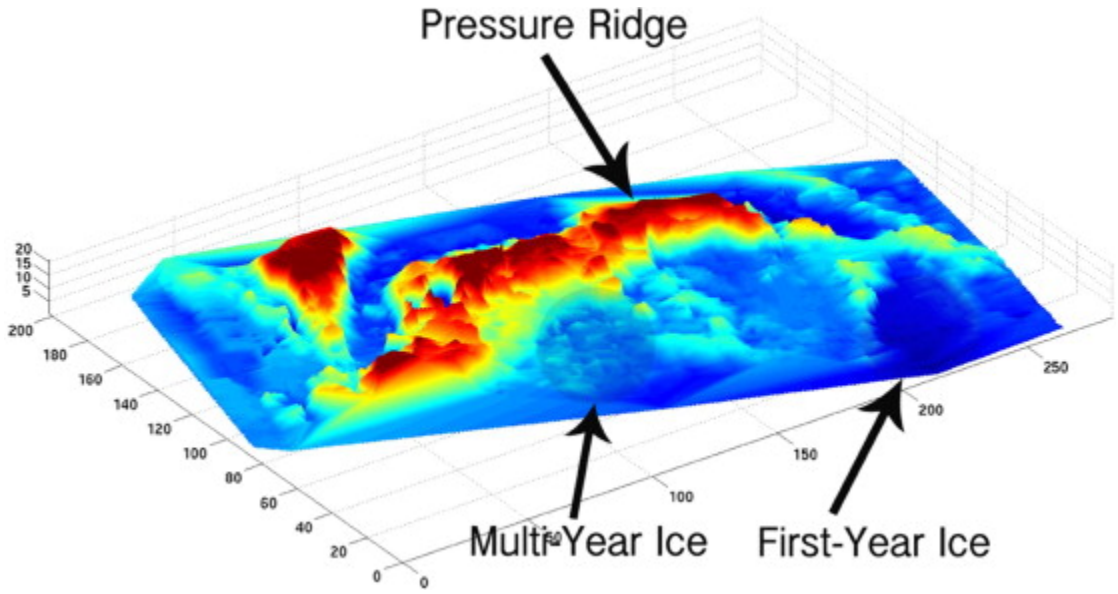

Figure 22. Side scan sonar imaging of a pressure ridge.

Finally, it should be noted that the time scale with which the data was collected may have added to errors in the overall assembly of the 3-D model. As surface ice conditions are only available on a weekly basis, the data was assembled similarly. If a surface condition matched the '7,10,12' classification, then all drafts for that same, weeklong time period were collected. It may be that the floes changed ice regime during the week, but that change was lost due to the insensitive nature of the surface condition reports. If available through another source, it would be curious to obtain daily imagery, and reassess the draft distributions with a tighter time frame.

7 Future Work

Exploring the method for quantifying storage capacity beneath sea ice highlights a number of areas where further study is necessary. From a theoretical perspective, storage space is intrinsically tied to subsurface roughness, for which no clear definition exists. That definition, though, is tied to a better understanding of the relative distribution of sea ice drafts. While this thesis focused on a single observed ice condition, the bimodality of the draft data inspires further research. It is important for future model development to understand if all ice conditions follow a bimodal exponential distribution, or if that is a characteristic of older, first year ice.

Following ice draft distributions, the influence of geography may also play an important role. In a paper by Arneborg (2017), research indicates that sea ice in the Baltic is dissimilar to Arctic ice because of high vessel traffic. High vessel traffic causes increased local ice deformation and affects draft development. This is further indication that maximum ice draft could depend on the local influences. So far, ice drafts, as related to storage capacity, have been studied in isolation, and without consideration of the external factors that might play a role.

If a general approach to describing sea ice can be established, then research can begin to approach the challenge of more accurately quantifying subsurface storage capacity over a given domain. There are persistent questions regarding the application of the equation proposed by LeShack and Chang (1977). That equation was predicated upon a normally distributed population of ice drafts and was developed using two-dimensional data sets. Instead of an arithmetic mean, the geometric mean might be used. Perhaps some measure between the two is most applicable. Regardless, the distribution should drive the definition, not an assumption about the nature of the drafts.

Historically, storage capacity has also been calculated by the use of a two-dimensional measure that is applied to three dimensions. As illustrated in this thesis, there are disparities in that approach. A two-dimensional measure overestimates the general quantity of ice; which underestimates the volume total for pooling. This overestimation would be compounded in a dynamic model. In a dynamic model, oil slicks are influenced by gravity which encourages oil to move from deeper regions to shallower regions. Extra ice would negatively impact proper modeling capabilities. It is critical for better modeling to understand how the capacity beneath the ice should be calculated.

Focusing on modeling, it was the intent that this thesis act as a stepping stone toward a dynamic sea ice subsurface model. While much of Chapter 4 was focused on those areas that would be enhanced by a better understanding of sea ice geometry in 3-D. As some of these topics were not related to the methodology here, they are related to follow up research for the future. Case in point, current models exist for sea ice from a climatological and oceanographic vantage point, but a dynamic subsurface model does not appear to exist. A subsurface sea ice model would allow for better investigation of the unique hydrodynamics characteristics occurring at the water-ice interface.

Some of those hydrodynamic characteristics would be the development of thermal and velocity boundary layers, and the momentum layer thickness along the water-ice interface. In theory, boundary layers develop when surface roughness changes, and expand infinitely outward into the water column. Beneath sea ice, though, the ice roughness is consistently varying, ice drafts protrude and impede the layer, and saline concentrations are extremely high near the surface of growing ice. The impact of these three attributes on the different boundary layers is not well understood, partially because modeling work is still in its infancy.

Preliminary work by McPhee (1976) suggests that the velocity boundary layer between water and ice is 2-4 meters deep and constrained by stratified flow. However, that supposition was developed by hand drilling a line of boreholes into the sea ice, then taking local velocity measurements. As those 2-D measurements were performed without any awareness of the surrounding ice profiles, it is easy to conceive that nearby pressure ridges, or other large keels, could have impacted the velocity boundary layer. Again, the influence of subsurface sea ice roughness impacts the proper understanding of subsurface dynamics.

Finally, classical approaches to boundary layers assume static pressure throughout that layer, with modest boundary layer surface curvature in the flow direction. Whether that is a valid assumption for rough ice remains to be explored. The shape of that flow profile and the pressure gradient within the boundary layer are likely subject to the influence of the ice roughness, and the geometry of the ice nearby. There is also the impact of fluid motion through bring channels that may affect the pressure gradient. If that pressure gradient isn't consistent, the dynamics of oil movement beneath the ice may also be impacted. All of these various avenues for future work solidify the critical need for a proper subsurface roughness definition, and better methodology for calculating storage capacity.

References

Andreas, E. L., Lange, M. A., Ackley, S. F., & Wadhams, P. (1993). Roughness of Weddell Sea ice and estimates of the air-ice drag coefficient. *Journal of Geophysical Research: Oceans*, *98*(C7), 12439-12452.

ARCUS. (2019). *Arctic Ambitions: Captain Cook and the Northwest Passage*. [online] Available at: https://www.arcus.org/witness-the-Arctic/2015/2/article/23159 [Accessed 10 Jun. 2019].

Arneborg, L., Höglund, A., Axell, L., Lensu, M., Liungman, O., & Mattsson, J. (2017). Oil drift modeling in pack ice–Sensitivity to oil-in-ice parameters. *Ocean Engineering*, *144*, 340-350. DOI: 10.1016/j.oceaneng.2017.09.041

ASL Environmental Sciences Inc. (2011). *IPS Processing Toolbox User's Guide.* Report by ASL Environmental Sciences Inc., Victoria BC Canada.

Afenyo, M., Veitch, B., & Khan, F. (2016). A state-of-the-art review of fate and transport of oil spills in open and ice-covered water. *Ocean Engineering*, *119*, 233-248. DOI: 10.1016/j.oceaneng.2015.10.014

Boufadel, M. C., Cui, F., Katz, J., Nedwed, T., & Lee, K. (2018). On the transport and modeling of dispersed oil under ice. *Marine pollution bulletin*, *135*, 569-580. DOI: 10.1016/j.marpolbul.2018.07.046

Bureau of Ocean and Energy Management (BOEM), *GCS NAD 83 Alaska Albers Projection*. 2015. [cited 25 March 2019]. Available from: https://www.boem.gov/uploadedFiles/BOEM/About_BOEM/BOEM_Regions/Alaska_Region/Leasing_and_Plans/Plans/Map%202.pdf

Comfort, G., & Purves, W. (1982). Behaviour of Crude Oil Spilled Under Multi-Year Ice. *EPS 4-EC-82-4 August 1982. Environment Canada, Environmental Protection Service, Ottawa(Ontario). 76 p, 9 Fig, 8 Tab, 6 Ref, 3 Append.*

Cox, J. C., & Schultz, L. A. (1981, March). The containment of oil spilled under rough ice. In *International Oil Spill Conference* (Vol. 1981, No. 1, pp. 203-208). American Petroleum Institute.

Doble, M. J., Skourup, H., Wadhams, P., & Geiger, C. A. (2012). C00E03 The relation between Arctic sea ice surface elevation and draft: A case study using coincident AUV sonar and airborne scanning laser (doi 10.1029/2011JC007076). *Journal of Geophysical Research-Part C-Oceans*, *117*(8).

Fingas, M. F., & Hollebone, B. P. (2003). Review of behaviour of oil in freezing environments. *Marine pollution bulletin*, *47*(9-12), 333-340. DOI: 10.1016/s0025-326x(03)00210-8

Fissel, D. B., Marko, J. R., & Melling, H. (2008). Advances in upward looking sonar technology for studying the processes of change in Arctic Ocean ice climate. *Journal of Operational Oceanography*, *1*(1), 9-18.

Frazier, K., & Ravens, T. (2019). Oil beneath Arctic Ice: Predicting Under-Ice Storage Capacity as a Means to Better Anticipate Oil Slick Spreading under Ice. In *Cold Regions Engineering 2019* (pp. 263-270). Reston, VA: American Society of Civil Engineers. DOI: 10.1061/9780784482599.031

Fukamachi, Y., Simizu, D., Ohshima, K. I., Eicken, H., Mahoney, A. R., Iwamoto, K., ... & Nihashi, S. (2017). Sea-ice thickness in the coastal northeastern Chukchi Sea from moored ice-profiling sonar. *Journal of glaciology*, *63*(241), 888-898. DOI: 10.1017/jog.2017.56

Gaver, D. P., & Jacobs, P. A. (1982). *Data Analysis and Modeling of Arctic Sea Ice Subsurface Roughness* (No. NPS55-82-031). NAVAL POSTGRADUATE SCHOOL MONTEREY CA.

Glaeser, J. L., & Vance, G. P. (1971). *A study of the behavior of oil spills in the Arctic*. COAST GUARD WASHINGTON DC APPLIED TECHNOLOGY DIV.

Harder, M. (1997). Roughness, age and drift trajectories of sea ice in large-scale simulations and their use in model verifications. *Annals of Glaciology*, *25*, 237-240.

Harder, M., Lemke, P., & Hilmer, M. (1998). Simulation of sea ice transport through Fram Strait: Natural variability and sensitivity to forcing. *Journal of Geophysical Research: Oceans*, *103*(C3), 5595-5606.

Hoult, D. P., Wolfe, S., O'Dea, S., & Patureau, J. P. (1975). *Oil in the Arctic*. MASSACHUSETTS INST OF TECH CAMBRIDGE.

Kovacs, A. (1977, January). Sea ice thickness profiling and under-ice oil entrapment. In *Offshore Technology Conference*. Offshore Technology Conference.

Kwok, R., & Untersteiner, N. (2011). The thinning of Arctic sea ice. *Phys. Today*, *64*(4), 36-41.

LeSchack, L. A., & Chang, D. C. (1977). *Arctic Under-Ice Roughness*. DEVELOPMENT AND RESOURCES TRANSPORTATION CO SILVER SPRING MD.

LeSchack, L. A. (1980). *Correlation of Under-Ice Roughness with Satellite and Airborne Thermal Infrared Data* (No. TR-2). LESCHACK ASSOCIATES LTD SILVER SPRING MD.

Lu, P., Li, Z., Cheng, B., & Leppäranta, M. (2011). A parameterization of the ice-ocean drag coefficient. *Journal of Geophysical Research: Oceans*, *116*(C7).

Maslowski, W., & Lipscomb, W. H. (2003). High resolution simulations of Arctic sea ice, 1979–1993. *Polar Research*, *22*(1), 67-74.

McPhee, M. G., & Smith, J. D. (1976). Measurements of the turbulent boundary layer under pack ice. *Journal of Physical Oceanography*, *6*(5), 696-711.

Melling, H., Johnston, P. H., & Riedel, D. A. (1995). Measurements of the underside topography of sea ice by moored subsea sonar. *Journal of Atmospheric and Oceanic Technology*, *12*(3), 589-602.

Montgomery, D. C., & Runger, G. C. (2014). *Applied statistics and probability for engineers*. John Wiley & Sons

Mudge, T.D., Fissel, D.B., Barrette, J., Sadowy, D., Borg, K., Billenness, D., Wolf, M., Bryce, A., Slonimer, A., Milutinovic, N., Lim, J., Lawrence, J., & Martinez, M. (2014). *Analysis of Ice and Metocean Measurements, Beaufort Sea 2012-2013, for Shell*. Project Report for Shell International Exploration and Production Inc., Houston, Texas by ASL Environmental Sciences Inc., Victoria, B.C. Canada. 14-24.

Nunez, C. (2016). *A Luxury Cruise Liner Is About to Sail the Arctic's Northwest Passage*. [online] News.nationalgeographic.com. Available at: https://news.nationalgeographic.com/2016/08/crystal-serenity-luxury-cruise-Arctic-northwest-passage/ [Accessed 10 Jun. 2019].

Oikkonen, A., & Haapala, J. (2011). Variability and changes of Arctic sea ice draft distribution–submarine sonar measurements revisited. *The Cryosphere*, *5*(4), 917-929. DOI: 10.5194/tc-5-917-2011.

Puskas, J., McBean, E., & Kouwen, N. (1987). Behaviour and transport of oil under smooth ice. *Canadian Journal of Civil Engineering*, *14*(4), 510-518.

Rothrock, D. A., & Thorndike, A. S. (1980). Geometric properties of the underside of sea ice. *Journal of Geophysical Research: Oceans*, *85*(C7), 3955-3963.

Schetz, J. A. (1984). *Foundations of boundary layer theory for momentum, heat, and mass transfer*. Inc. Englewood Cliffs: Prentice-Hall. 9-10, 141-155.

Steiner, N., Harder, M., & Lemke, P. (1999). Sea-ice roughness and drag coefficients in a dynamic–thermodynamic sea-ice model for the Arctic. *Tellus A*, *51*(5), 964-978. DOI: 10.3402/tellusa.v51i5.14505

Timco, G. W., & Weeks, W. F. (2010). A review of the engineering properties of sea ice. *Cold regions science and technology*, *60*(2), 107-129. DOI: 10.1016/j.coldregions.2009.10.003

Thorndike, A. S., & Colony, R. (1982). Sea ice motion in response to geostrophic winds. *Journal of Geophysical Research: Oceans*, *87*(C8), 5845-5852.

Valenti, V. A. (2015). *Sea ice parameters for actions on offshore structures in the Beaufort and Chukchi Seas* (Doctoral dissertation, University of Alaska Anchorage).

Venkatesh, S., El-Tahan, H., Comfort, G., & Abdelnour, R. (1990). Modelling the behaviour of oil spills in ice-infested waters. *Atmosphere-Ocean*, *28*(3), 303-329. DOI: 10.1080/07055900.1990.9649380

Wadhams, P., Wilkinson, J. P., & McPhail, S. D. (2006). A new view of the underside of Arctic sea ice. *Geophysical Research Letters*, *33*(4).

Wadhams, P., Hughes, N., & Rodrigues, J. (2011). Arctic sea ice thickness characteristics in winter 2004 and 2007 from submarine sonar transects. *Journal of Geophysical Research: Oceans*, *116*(C8).

Wadhams, P., & Toberg, N. (2012). Changing characteristics of arctic pressure ridges. *Polar Science*, *6*(1), 71-77. DOI: 10.1016/j.polar.2012.03.002

Waldie, P. (2014). A reality check on the Northwest Passage 'boom,'. *The Globe and Mail*. Available at: https://www.theglobeandmail.com/report-on-business/breakthrough/will-cold-dark-northwest-passage-see-more-ships/article16231502/ [Accessed 10 Jun. 2019].

Weisstein, Eric W. (2019) "Geometric Mean." From *MathWorld*--A Wolfram Web Resource. http://mathworld.wolfram.com/GeometricMean.html

Wilkinson, J., Wadhams, P., & Hughes, N. (2007). Modelling the spread of oil under fast sea ice using three-dimensional multibeam sonar data. *Geophysical Research Letters*, *34*(22). doi: 10.1029/2007gl031754

World Meteorological Organization. (1970). *WMO Sea-ice Nomenclature: Terminology, Codes, Illustrated Glossary and Symbols*. Secretariat of the World Meteorological Organization.

Yang, M., Khan, F., Garaniya, V., & Chai, S. (2015). Multimedia fate modeling of oil spills in ice-infested waters: An exploration of the feasibility of fugacity-based approach. *Process Safety and Environmental Protection*, *93*, 206-217. DOI: 10.1016/j.psep.2014.04.009

Yapa, P. D., & Chowdhury, T. (1990). Spreading of oil spilled under ice. *Journal of Hydraulic Engineering*, *116*(12), 1468-1483.

Zelenke, B., O'Connor, C., Barker, C. H., Beegle-Krause, C. J., & Eclipse, L. (2012). General NOAA operational modeling environment (GNOME) technical documentation

Appendix A

Beaufort Surface Data

Ice Egg Code	1	2	3	4	5	6	7	8
Thickness (cm)	0-10	10-30.	10-15.	15-30.	15-30.	30-200.	30-70.	30-70.
Description:	New, Frazil, Slush, etc	Nilas, Ice Rind	Young	Gray	Gray - White	1Y	1Y, thin	1Y, thin, stage 1
Location Nickname:	SiteA (ADCP)							
Latitude:	70d 21.982' N							
Longitude:	146d 0.009' W							
DateRange:	10/2010 - 6/18/2011							
				Ice Egg Data				
Date:	Sa	Sb	Sc	Combined S	Storage	Concentration	Assumed C.	QC
10/1/10	fast			fast				
10/8/10	fast			fast				
10/15/10	1	0	0	1,0,0		5,7	60	
10/22/10	1	0	0	1,0,0		1,2	15	
10/29/10	3	1	0	3,1,0		7,10	85	
11/5/10	3	1	0	3,1,0		6,8	70	
11/12/10	3	1	7	3,1,7		6,9	75	
11/19/10	fast			fast				
11/26/10	fast			fast				
12/3/10	fast			fast				
12/10/10	fast			fast				
12/17/10	fast			fast				
12/24/10	fast			fast				
12/31/10	fast			fast				
1/7/11	fast			fast				
1/14/11	fast			fast				
1/21/11	fast			fast				
1/28/11	fast			fast				
2/4/11	fast			fast				
2/11/11	fast			fast				
2/18/11	fast			fast				
2/25/11	fast			fast				
3/4/11	fast			fast				
3/11/11	fast			fast				
3/18/11	fast			fast				
3/25/11	fast			fast				
4/1/11	fast			fast				
4/8/11	fast			fast				
4/15/11	fast			fast				
4/22/11	fast			fast				
4/29/11	fast			fast				
5/6/11	fast			fast				
5/13/11	fast			fast				
5/20/11	fast			fast				
5/27/11	fast			fast				
6/3/11	fast			fast				
6/10/11	fast			fast				
6/17/11	fast			fast				
6/24/11	fast			fast				
7/1/11	7	3	1	7,3,1		6,9	75	
7/8/11	1	3	7	1,3,7		4,6	50	
7/15/11	1	3	7	1,3,7		4,6	50	
7/22/11	1	3	7	1,3,7		2,4	30	
7/29/11	1	3	7	1,3,7		1,2	15	
8/5/11	1	3	7	1,3,7		1,2	15	
8/12/11	1	3	0	1,3,0		1,2	15	
8/19/11	ice free							
8/26/11	ice free							
9/2/11	ice free							
9/9/11	ice free							
9/16/11	ice free							
9/23/11	ice free							
9/30/11	ice free							

9	10	11	12	13	14
30-70.	70-120.	>120	>2m	>2m	>2m
as displayed on AOOS:	1*	4*	7*	8*	9*
1Y, thin, stage 2	1Y Ice, med	1Y ice, thick	Old 1Y ice	SY ice	MY ice

Location Nickname:	Site A (ADCP)		
Latitude:	70d 21.982' N	* recovered/deployed 10/1/2011	
Longitude:	146d 0.009' W	* battery died june 18th, 2012	
Date Range:	10/1/2011-10/2012	*ADCP found to be 11min 23sec slow at recovery	

Ice Egg Data

Date:	Sa	Sb	Sc	Combined S	Storage	Concentration	Assumed C.	QC
10/1/11	ice free							
10/8/11	ice free							
10/15/11	1	0	0	1,0,0		3,5	40	
10/22/11	1	0	0	1,0,0		6,8	70	
10/29/11	1	3	0	1,3,0		7,9	80	
11/5/11	1	3	0	1,3,0		6,8	70	
11/12/11	1	3	0	1,3,0		6,9	75	
11/19/11	fast							
11/26/11	fast							
12/3/11	fast							
12/10/11	fast							
12/17/11	fast							
12/24/11	fast							
12/31/11	fast							
1/7/12	fast							
1/14/12	10	7	0	10,7,0		8,10	90	
1/21/12	10	7	11	10,7,11		8,10	90	
1/28/12	fast							
2/4/12	fast							
2/11/12	fast							
2/18/12	fast							
2/25/12	fast							
3/3/12	fast							
3/10/12	fast							
3/17/12	fast							
3/24/12	fast							
3/31/12	fast							
4/7/12	fast							
4/14/12	fast							
4/21/12	fast							
4/28/12	fast							
5/5/12	fast							
5/12/12	fast							
5/19/12	fast							
5/26/12	fast							
6/2/12	fast							
6/9/12	fast							
6/16/12	fast							
6/23/12	7	3	1	7,3,1		6,9	75	
6/30/12	7	3	1	7,3,1		6,9	75	
7/7/12	3	1	7	3,1,7		6,8	70	
7/14/12	7	10	11	7,10,11		6,9	75	
7/21/12	7	10	11	7,10,11		5,7	60	
7/28/12	3	6	1	3,6,1		6,9	75	
8/4/12	3	6	1	3,6,1		6,8	70	
8/11/12	3	1	7	3,1,7		5,7	60	
8/18/12	SIF							
8/25/12	SIF							
9/1/12	SIF							
9/8/12	SIF							
9/15/12	SIF							
9/22/12	SIF							
9/29/12	SIF							
10/6/12	SIF							

Location Nickname:	Site A (ADCP)							
Latitude:	70d 22.002'N							
Longitude:	145d 59.978' W							
Date Range:	10/6/2012 -10/1/2013							
				Ice Egg Data				
Date:	Sa	Sb	Sc	Combined S	Storage	Concentration	Assumed C.	QC
10/6/12	SIF							
10/13/12	1	0	0	1,0,0		2,4	30	
10/20/12	1	3	0	1,3,0		6,8	70	
10/27/12	1	3	0	1,3,0		7,9	80	
11/3/12	1	3	0	1,3,0		7,9	80	
11/10/12	3	1	0	3,1,0		7,9	80	
11/17/12	3	1	0	3,1,0		7,9	80	
11/24/12	3	1	0	3,1,0		7,9	80	
12/1/12	3	7	1	3,7,1		8,10	90	
12/8/12	3	7	1	3,7,1		8,10	90	
12/15/12	7	3	0	7,3,0		8,10	90	
12/22/12	10	7	11	10,7,11		8,10	90	
12/29/12	10	7	11	10,7,11		8,10	90	
1/5/13	10	7	11	10,7,11		8,10	90	
1/12/13	10	7	11	10,7,11		8,10	90	
1/19/13	FAST							
1/26/13	7	10	3	7,10,3		7,10	85	
2/2/13	10	11	7	10,11,7		7,10	85	
2/9/13	10	11	7	10,11,7		8,10	90	
2/16/13	10	11	7	10,11,7		8,10	90	
2/23/13	10	11	7	10,11,7		8,10	90	
3/2/13	FAST							
3/9/13	FAST							
3/16/13	FAST							
3/23/13	FAST							
3/30/13	11	10	12	11,10,12		8,10	90	
4/6/13	11	10	12	11,10,12		8,10	90	
4/13/13	10	11	12	10,11,12		7,10	85	
4/20/13	10	11	12	10,11,12		7,10	85	
4/27/13	10	11	12	10,11,12		7,10	85	
5/4/13	10	11	12	10,11,12		7,10	85	
5/11/13	10	1	7	10,1,7		6,8	70	
5/18/13	10	1	7	10,1,7		7,10	85	
5/25/13	10	1	7	10,1,7		7,10	85	
6/1/13	1	3	7	1,3,7		5,7	60	
6/8/13	SIF							
6/15/13	7	3	10	7,3,10		6,9	80	
6/22/13	10	11	7	10,11,7		7,10	85	
6/29/13	1	3	7	1,3,7		2,4	30	
7/6/13	1	3	7	1,3,7		5,7	60	
7/13/13	1	3	7	1,3,7		2,4	30	
7/20/13	1	3	7	1,3,7		1,3	20	
7/27/13	SIF							
8/3/13	1	3	7	1,3,7		1,3	20	
8/10/13	3	1	12	3,1,12		1,3	20	
8/17/13	SIF							
8/24/13	SIF							
8/31/13	SIF							
9/7/13	SIF							
9/14/13	SIF							
9/21/13	SIF							
9/28/13	SIF							
10/5/13	SIF							

Appendix B

Chukchi Surface Data

	Ice Egg Data							
Date:	Sa	Sb	Sc	Combined S	Storage	Concentration	Assumed C.	QC
11/8/10	3	1	0	3,1,0	6482.73936	60-90	75	1.21466931
11/15/10	3	7	1	3,7,1	2062.88278	60-90	75	1.62084221
12/6/10	3	1	7	3,1,7	2894.38375	60-80	70	1.04460613
12/13/10	3	7	1	3,7,1	14614.1209	70-90	80	4.69385304
12/20/10	7	3	1	7,3,1	8639.43624	70-90	80	2.30507146
12/27/10	7	3	12	7,3,12	14974.3712	70-100	85	12.7357868
1/3/11	7	3	12	7,3,12	41753.2849	70-100	85	4.45004055
1/10/11	7	3	12	7,3,12	22030.5907	70-100	85	1.14736457
1/17/11	7	3	12	7,3,12	8230.16323	70-100	85	1.34266899
1/24/11	7	10	12	7,10,12	9865.6049	70-100	85	2.39310241
1/31/11	7	10	3	7,10,3	40577.449	70-100	85	1.26278063
2/7/11	7	10	3	7,10,3	22226.6273	70-100	85	2.17454202
2/14/11	7	10	3	7,10,3	51806.7443	70-100	85	1.30336221
2/21/11	10	7	3	10,7,3	56473.3661	70-100	85	1.16111308
2/28/11	10	7	3	10,7,3	31197.7955	70-100	85	1.04992899
3/7/11	F8				17049.4049			1.53207974
3/14/11	F8				16136.9814			2.44443529
3/21/11	F8				31124.9873			1.54371485
3/28/11	F9				27959.7617			1.50039382
4/4/11	7	10	12	7,10,12	25784.0202	70-100	85	1.45210825
4/11/11	7	10	12	7,10,12	28536.6758	70-100	85	1.59963505
4/18/11	7	10	12	7,10,12	30802.5118	70-100	85	1.93239654
4/25/11	7	10	12	7,10,12	27979.1999	70-90	80	1.65626602
5/2/11	7	10	12	7,10,12	14383.6049	80-100	90	1.83466309
5/9/11	7	10	12	7,10,12	45389.8092	80-100	90	1.04803745
5/16/11	7	10	12	7,10,12	43238.2229	80-100	90	1.27601248
5/23/11	7	10	12	7,10,12	32750.6088	80-100	90	1.49948043
5/30/11	7	10	12	7,10,12	11069.8884	80-100	90	1.7023476
6/6/11	3	7	1	3,7,1	67308.3211	10-30	20	1.01958204
6/13/11	3	1	7	3,1,7	4838.38854	10-30	20	1.00612172

	Ice Egg Data							
Date:	Sa	Sb	Sc	Comined S	Storage	Concentration	Assumed C.	QC
11/22/11	1	0	0	1,0,0	958.79495	50-70	60	1.11435425
11/29/11	3	1	7	3,1,7	1305.44604	60-80	70	1.13559505
12/6/11	7	3	10	7,10,3	2018.4538	70-100	85	1.35024352
12/13/11	7	3	10	7,10,3	13008.0182	70-100	85	1.40718541
12/20/11	7	3	10	7,10,3	16970.2083	70-100	85	1.12153241
12/27/11	7	10	0	7,10,0	38226.6302	70-100	85	1.10438969
1/3/12	7	10	0	7,10,0	11858.2241	70-100	85	1.26043636
1/10/12	10	12	11	10,12,11	19800.1602	90-100	95	1.18084064
1/17/12	10	12	11	10,12,11	10360.1932	90-100	95	1.68302339
1/24/12	11	12	10	11,12,10	24183.2247	90-100	95	3.55249275
1/31/12	11	12	10	11,12,10	13293.4175	90-100	95	3.31648464
2/7/12	11	12	10	11,12,10	46693.716	90-100	95	3.16719304
2/14/12	11	12	10	11,12,10	24142.1672	90-100	95	1.10570891
2/21/12	11	12	10	11,12,10	10900.0726	90-100	95	1.55595015
2/28/12	11	12	10	11,12,10	13316.6173	90-100	95	1.14934613
3/6/12	11	12	10	11,12,10	3166.98776	70-100	85	1.8585093
3/13/12	11	12	10	11,12,10	1520.62753	70-100	85	1.25992659
3/20/12	10	11	7	10,11,7	22651.025	70-100	85	1.0176975
3/27/12	10	12	7	10,11,7	9434.58495	70-100	85	1.79042976
4/3/12	11	12	10	11,12,10	19869.8621	80-100	90	1.91181665
4/10/12	10	12	7	10,12,7	45446.3293	70-100	85	1.16636235
4/17/12	10	12	7	10,12,7	14142.4155	70-100	85	2.01278667
4/24/12	10	12	7	10,12,7	30813.8416	70-100	85	1.20521886
5/1/12	10	12	7	10,12,7	31054.031	70-100	85	2.12716698
5/8/12	10	12	7	10,12,7	36327.8957	70-100	85	1.63489559
5/15/12	10	12	7	10,12,7	59003.2435	70-100	85	1.06082298
5/22/12	10	12	7	10,12,7	37180.8411	70-90	80	4.82432791
5/29/12	10	12	7	10,12,7	27649.0965	70-90	80	1.13083189
6/5/12	10	7	12	10,7,12	28714.2969	60-90	75	1.50186821
6/12/12	10	7	12	10,7,12	59184.3754	60-90	75	1.38488224
6/19/12	10	7	12	10,7,12	37458.0061	60-90	75	1.03000213
6/26/12	10	7	12	10,7,12	72474.6373	60-80	70	1.84967389
7/3/12	10	7	12	10,7,12	15963.6041	60-90	75	1.26243579
7/10/12	7	3	1	7,3,1	17318.7571	60-90	75	1.05236841
7/24/12	7	3	1	7,3,1	488.164216	30-50	40	1.08481739
7/31/12	3	7	10	3,7,10	67.460428	60-80	70	1.02366085

	Ice Egg Data							
Date:	Sa	Sb	Sc	Combined S	Storage	Concentration	Assumed C	QC
11/8/12	1	3	0	1,3,0	5.78361529	30-50	40	1.39589562
11/15/12	3	7	1	3,7,1	2215.26642	70-90	80	1.93732901
11/22/12	7	3	1	7,3,1	3190.01943	70-90	80	1.42152875
11/29/12	7	3	1	7,3,1	4113.4646	80-100	90	1.24204635
12/6/12	7	3	1	7,3,1	4869.33075	80-100	90	1.10867129
12/13/12	7	3	0	7,3,0	8264.76572	80-100	90	9.65707177
12/20/12	7	3	10	7,3,10	15124.3636	80-100	90	1.68667502
12/27/12	7	10	3	7,10,3	22956.1691	70-100	85	1.15465219
1/3/13	7	10	3	7,10,3	21275.558	70-100	85	1.17382209
1/10/13	10	7	11	10,7,11	35087.9125	70-100	85	1.13730574
1/17/13	10	7	11	10,7,11	47057.4555	80-100	90	1.11726671
1/24/13	10	7	11	10,7,11	26195.6526	70-100	85	1.13135197
1/31/13	10	11	7	10,11,7	6623.19539	70-100	85	1.32271887
2/7/13	11	12	10	11,12,10	13758.01	80-100	90	1.15768778
2/14/13	10	11	7	10,11,7	9915.28998	80-100	90	1.03573228
2/21/13	10	11	7	10,11,7	13853.41	80-100	90	1.04665117
2/28/13	10	11	7	10,11,7	31922.8134	80-100	90	1.40773939
3/7/13	11	10	7	11,10,7	77896.8884	80-100	90	1.0571293
3/14/13	10	7	12	10,7,12	90322.148	70-100	85	1.35900989
3/21/13	10	7	12	10,7,12	27602.077	70-100	85	5.97721499
3/28/13	11	10	7	11,10,7	22585.1826	70-100	85	1.1239751
4/4/13	11	10	0	11,10,0	31546.6798	80-100	90	1.1547324
4/11/13	11	10	7	11,10,7	28330.8646	70-100	85	1.91469858
4/18/13	11	10	12	11,10,12	12578.144	70-100	85	2.16165184
4/25/13	11	10	12	11,10,12	22720.2939	70-100	85	1.51258499
5/2/13	11	10	12	11,10,12	20071.8971	80-100	90	2.1677257
5/9/13	11	10	12	11,10,12	34776.9443	80-100	90	1.13237139
5/16/13	7	10	12	7,10,12	38769.601	70-90	80	2.54611483
5/23/13	7	10	12	7,10,12	69049.7746	70-100	85	1.61838847
5/30/13	7	10	12	7,10,12	19305.8927	70-100	85	1.43295898
6/6/13	7	10	12	7,10,12	39108.8765	70-100	85	5.29262802
6/13/13	7	10	12	7,10,12	85191.1054	70-100	85	1.03370978
6/20/13	7	10	3	7,10,3	21233.6389	70-100	85	1.19101204
6/27/13	7	3	10	7,3,10	17885.0819	70-90	80	1.28811824
7/4/13	3	7	1	3,7,1	1384.71258	60-90	75	1.07401306

	Ice Egg Data							
Date:	Sa	Sb	Sc	Combined S	Storage	Concentration	Assumed C.	QC
11/20/2013	1	0	0	1,0,0	2865.29988	40-60	50	1.17529161
11/27/2013	7	3	1	7,3,1	9882.32809	70-90	80	2.48895793
12/4/2013	1	3	7	1,3,7	701.108724	50-70	60	1.71315331
12/11/2013	7	3	12	7,3,12	4963.61906	70-100	85	1.25270808
12/18/2013	7	3	12	7,3,12	8517.61524	70-100	85	2.75278453
12/25/2013	10	7	12	10,7,12	15004.6782	70-90	80	2.92343697
1/1/2014	10	7	12	10,7,12	13261.809	70-90	80	1.07462567
1/8/2014	7	3	10	7,3,10	22073.6932	70-90	80	1.3499666
1/15/2014	10	7	3	10,7,3	31402.2224	70-100	85	1.26452437
1/22/2014	10	7	3	10,7,3	91440.2867	70-100	85	1.27664145
1/29/2014	10	7	3	10,7,3	47311.3646	70-100	85	1.160893
2/5/2014	10	7	3	10,7,3	47206.0388	70-100	85	2.29747546
2/12/2014	10	7	3	10,7,3	37580.665	70-100	85	3.33182356
2/19/2014	10	7	3	10,7,3	34898.5054	70-100	85	1.1328857
2/26/2014	10	7	3	10,7,3	43192.3193	70-100	85	1.8421603
3/5/2014	10	7	3	10,7,3	21928.7963	80-100	90	1.24330903
3/12/2014	10	7	3	10,7,3	31982.3576	80-100	90	1.05072134
3/19/2014	10	7	3	10,7,3	34429.2036	70-100	85	1.19824505
3/26/2014	10	7	3	10,7,3	28201.4458	70-100	85	1.10128539
4/2/2014	10	7	3	10,7,3	15676.1444	70-100	85	3.43020994
4/9/2014	10	7	3	10,7,3	20739.4285	80-100	90	1.14353626
4/16/2014	10	7	3	10,7,3	21079.3563	80-100	90	2.26370247
4/23/2014	10	7	3	10,7,3	18541.4317	80-100	90	1.48872048
4/30/2014	10	7	3	10,7,3	69683.3873	80-100	90	1.23423949
5/7/2014	10	7	3	10,7,3	56385.0272	80-100	90	1.23172176
5/14/2014	10	7	3	10,7,3	55793.4157	80-100	90	1.05846132
5/21/2014	10	7	12	10,7,12	31535.4135	80-100	90	1.70834346
5/28/2014	10	7	12	10,7,12	36412.2739	80-100	90	1.22938038
6/4/2014	10	7	12	10,7,12	76.6018486	80-100	90	1.00007879
6/11/2014	10	7	12	10,7,12	23551.1195	80-100	90	3.89424828
6/18/2014	10	7	12	10,7,12	19369.3033	80-100	90	2.65432968
6/25/2014	10	7	12	10,7,12	379.25648	80-100	90	1.14192161
7/2/2014	10	7	12	10,7,12	218.050703	70-90	80	1.00005746
7/9/2014	7	10	12	7,10,12	459.437764	50-70	60	1.01747449

Appendix C

Matlab Code for Draft Measurements

```
% Kelsey Frazier
% University of Alaska Anchorage
% December 2019, Department of Mechanical Engineering

clc, clear

% ----------------- General Information ---------------------
%
% This code was written to import draft data from the North Slope Science Initiative,
% Remove data specific to a key set of observable surface conditions,
% Generate a histogram of the drafts for that surface conditions,
% Determine the appropriate probability density function,
% Generate a 3-D array of data based on the PDF, from which a surface will be generated
% in ArcGIS.
%
% Data for the Chukchi is available from:
% http://catalog.northslopescience.org/entries/8457
%
% Date for the Beaufort is available from:
% http://catalog.northslopescience.org/entries/8456
%
%
% ---------------- Loading Data -------------------------------
%
% Raw data is in the form of .dat files at the NSSI website. For this project,
% only data from the Chukchi site 'Crakerjack' and Beaufort 'Site A' were utilized.
% Other data is available but this program builds off prior efforts.
%
% Data comes in two formats: spatial and time series. The spatial data comes from the time
% series. Post processing took the time series and converted it into spatial measurements
% 1 meter in separation. This code uses the spatial series data.
%
% Spatial series data has either 5 or 7 columns.
%   Input: Regularly-spaced spatial series of:
%    (5 or 7)   idraft : ice draft (m)
%    (1)        t      : elapsed time (s) interpolated time of observation,
%    (2)        dist   : Distance (km double), should be 1 m
%    (3)        dX     : Eastward component of ice drift, DisplX (km double)
%    (4)        dY     : Northward component of ice drift, DisplX (km double)
%    (5 or 7)   dE     : Eastward component of ice drift, DisplE (km double) in some
%    datasets
%    (6)        dN     : Northward component of ice drift, DisplN (km double) in some
%    datasets
%
% This program only utilizes the date and draft measurements.
%
% ------------------------------------------------------------
%-------- START TIMES: manually input these -----------------
% ------------------------------------------------------------
```

```
% start times come from the header files for each data set
% for each year data was collected

starttime(1,:) = datetime(2010,10,15,0,3,53.896);
starttime(2,:) = datetime(2010,10,15,0,3,53.896);
starttime(3,:) = datetime(2010,12,1,0,5,36.395);
starttime(4,:) = datetime(2011,6,1,0,12,11.422);

% figure out how big the starttime matrix is
   n = length(starttime);

% generate a time matrix of zeros that you'll use for actual
% times later in the program

   timeUnix = zeros(1,n)';
   j = 1;

% convert all the starttimes to UNIX time
   while j <=4
      timeUnix(j,1) = posixtime(starttime(j));
      j = j+1;
   end

% ------------------------------------------------------------
% ------- load the data imported to the workspace ----------
% ------------------------------------------------------------

% at this point, you've used the built in function to import the draft data to matlab.
% Be sure to save the data to the workspace, so you can reload it as you need it.
% use the 'load' command to open the saved data if it isn't already open.

load('2010CJmatlab.mat');

% add the starttime to each element of the matrix
CJ10A = [CJ1011P3S1(:,1)+timeUnix(1) CJ1011P3S1(:,2)];
CJ10B = [CJ1011P3S2(:,1)+timeUnix(2) CJ1011P3S2(:,2)];
CJ10C = [CJ1011P4S3(:,1)+timeUnix(3) CJ1011P4S3(:,2)];
CJ10D = [CJ1011P5S3(:,1)+timeUnix(4) CJ1011P5S3(:,2)];

%% ------------------------------------------------------------------
% 7-10-12 ice observations come from the following weekly reports:
%       24-Jan-2011
%       4-Apr-2011 to 30-May-2011
%       16-May-2013 to 13-Jun-2013
%       9-Jul-2014
% Ice reports were given on a weekly basis up to 2015
% Consider all 7 days as the same ice condition for calculations
% ------------------------------------------------------------------

% give yourself a start and stop time range, in between which you'll
% tell matlab to go find draft data

alpha = posixtime(datetime('24-Jan-2011'));
```

```
beta = posixtime(datetime('30-jan-2011'));

gamma = posixtime(datetime('4-Apr-2011'));
sigma = posixtime(datetime('5-June-2011'));

epsilon = posixtime(datetime('16-May-2013'));
zeta = posixtime(datetime('19-Jun-2013'));

eta = posixtime(datetime('9-Jul-2014'));
theta = posixtime(datetime('25-Jun-2013'));

% given you've put your observed ice conditions into UNIX time; now search the data for
% draft data that falls into that category by counting the indicies that are within the date range

countA = 0;
countB = 0;
countC = 0;
countD = 0;
countE = 0;
countF = 0;

% check the first data set
for i = 1:length(CJ10A)
  if CJ10A(i,1) >= alpha & CJ10A(i,1) <= beta
     countA = countA + 1;
  end
end

% check the second data set
for i = 1:length(CJ10B)
  if CJ10B(i,1) >= alpha & CJ10B(i,1) <= beta
     countB = countB + 1;
  end
end

% check the third data set
for i = 1:length(CJ10C)
   if CJ10C(i,1) >= alpha & CJ10C(i,1) <= beta
     countC = countC + 1;
   elseif CJ10C(i,1) >= gamma & CJ10C(i,1) <= sigma
      countE = countE + 1;
   end
end

% check the fourth data set
for i = 1:length(CJ10D)
   if CJ10D(i,1) >= alpha & CJ10D(i,1) <= beta
     countD = countD + 1;
   elseif CJ10C(i,1) >= gamma & CJ10C(i,1) <= sigma
      countF = countF + 1;
  end
end
```

```
% Now that you've figured out where the data in the given range is located,
% make a new matrix with just those drafts, excluding the date because it's not needed
% for this analysis
% ------------------------------------------------------

draft2010A = zeros(countC,1);
draft2010B = zeros(countE,1);

for i = 1:length(CJ10C)
   if CJ10C(i,1) >= alpha & CJ10C(i,1) <= beta
      if CJ10C(i,2)>0
     draft2010A(i) = CJ10C(i,2);
      end
   elseif CJ10C(i,1) >= gamma & CJ10C(i,1) <= sigma
      if CJ10C(i,2)>0
      draft2010B(i) = CJ10C(i,2);
      end
   end
end

% make the 2010/2011 matrix of non zero draft measurements. Combine all the data points:
draft = [draft2010A; draft2010B];
% now remove only the non zero draft measurements
TenEleven = nonzeros(draft);
```

Now, go do this again for the other data sets. Then we combine those and do statistics voodoo

```
% ----------------------------------------
% Thesis code for the 2013 Data Set
%
% Other data sets computed in another file
%
% Uses the 2012 Data set
%
%
%
% ------------------------------------------------------------
%-------- START TIMES: manually input these -----------------
% ------------------------------------------------------------
% start times come from the header files for each data set
% for each year data was collected

starttime2(1,:) = datetime(2012,12,1,0,3,52.210);
starttime2(2,:) = datetime(2013,6,1,0,10,2.823);


% figure out how big the starttime matrix is
   n = length(starttime2);
```

```
% generate a time matrix of zeros that you'll use for actual
% times later in the program

   timeUnix = zeros(1,n)';
   j = 1;

% convert all the starttimes to UNIX time
   while j <=n
      timeUnix(j,1) = posixtime(starttime2(j));
      j = j+1;
   end

% ------------------------------------------------------------
% ------- load the data imported to the workspace ----------
% ------------------------------------------------------------

% at this point, you've used the built in function to import the draft data to matlab.
% Be sure to save the data to the workspace, so you can reload it as you need it.
% use the 'load' command to open the saved data if it isn't already open.

load('2013CJmatlab.mat');

% add the starttime to each element of the matrix
CJ13A = [CJ201307201208p04disted02seg03ASCII(:,1)+timeUnix(1)
CJ201307201208p04disted02seg03ASCII(:,2)];
CJ13B = [CJ201307201208p05disted02seg03ASCII(:,1)+timeUnix(2)
CJ201307201208p05disted02seg03ASCII(:,2)];

% give yourself a start and stop time range, in between which you'll
% tell matlab to go find draft data

epsilon = posixtime(datetime('16-May-2013'));
zeta = posixtime(datetime('19-Jun-2013'));

% given you've put your observed ice conditions into UNIX time; now search the data for
% draft data that falls into that category by counting the indicies that are within the date range

countA2 = 0;
countB2 = 0;

% check the first data set
for i = 1:length(CJ13A)
  if CJ13A(i,1) >= epsilon & CJ13A(i,1) <= zeta
     countA2 = countA2 + 1;
  end
end

% check the second data set
for i = 1:length(CJ13B)
  if CJ13B(i,1) >= epsilon & CJ13B(i,1) <= zeta
     countB2 = countB2 + 1;
  end
end
```

```
-----------------------------------------------------
% Now that you've figured out where the data in the given range is located,
% make a new matrix with just those drafts, excluding the date because it's not needed
% for this analysis
% ------------------------------------------------------

draft2013A = zeros(countA2,1);
draft2013B = zeros(countB2,1);

for i = 1:length(CJ13A)
   if CJ13A(i,1) >= epsilon & CJ13A(i,1) <= zeta
      if CJ13A(i,2)>0
         draft2013A(i) = CJ13A(i,2);
      end
   end
end

for i = 1:length(CJ13B)
   if CJ13B(i,1) >= epsilon & CJ13B(i,1) <= zeta
      if CJ13B(i,2)>0
         draft2013B(i) = CJ13B(i,2);
      end
   end
end

% make the 2010/2011 matrix of non zero draft measurements. Combine all the data points:
draft = [draft2013A; draft2013B];
% now remove only the non zero draft measurements
Thirteen = nonzeros(draft);
```

Now combine the sets and save

```
TotalDraft = [TenEleven' Thirteen'];
save('TotalDraft.mat', 'TotalDraft');
```

Appendix D

Distribution Fitting Data

```
% Check to see which distribution is the best fit

% take a sample of the total draft data:
sample = sort(datasample(TotalDraft,500,'Replace',false))';

pd1 = fitdist(sample, 'Weibull')
pd1 =
  WeibullDistribution

  Weibull distribution
    A = 2.74081   [2.53008, 2.96909]
    B = 1.15686   [1.08318, 1.23555]


[h1,p1,stats1] = chi2gof(sample,'CDF',pd1)

     h1 = 1


     p1 = 0.0014


stats1 = struct with fields:
    chi2stat: 17.6724
          df: 4
       edges: [0.0143 1.7159 3.4176 5.1192 6.8209 8.5226 10.2242 17.0309]
           O: [260 112 60 36 17 7 8]
           E: [220.5320 141.9479 73.7985 35.4076 16.1377 7.0795 5.0968]


pd2 = fitdist(sample, 'Exponential')
pd2 =
  ExponentialDistribution

  Exponential distribution
    mu = 2.59683   [2.38344, 2.84038]


[h2,p2,stats2] = chi2gof(sample,'CDF', pd2)

     h2 = 0


     p2 = 0.5731


stats2 = struct with fields:
    chi2stat: 3.8369
          df: 5
       edges: [0.0143 1.7159 3.4176 5.1192 6.8209 8.5226 10.2242 17.0309]
           O: [260 112 60 36 17 7 8]
           E: [241.7735 124.1308 64.4605 33.4740 17.3829 9.0268 9.7515]


pd3 = fitdist(sample,'lognormal')
pd3 =
```

```
  LognormalDistribution

  Lognormal distribution
       mu = 0.534105   [0.442543, 0.625666]
    sigma =  1.04207   [0.981234, 1.111]
```

```
[h3,p3,stats3] = chi2gof(sample,'CDF', pd3)
```

```
      h3 = 1


      p3 = 0.0105


stats3 = struct with fields:
    chi2stat: 14.9711
          df: 5
       edges: [0.0143 1.7159 3.4176 5.1192 6.8209 8.5226 10.2242 11.9259 17.0309]
           O: [260 112 60 36 17 7 4 4]
           E: [251.1180 122.6535 53.3196 27.0245 15.2177 9.2344 5.9257 15.5066]
```

Appendix E

Matlab Draft Creation

Make a mesh matrix

```
% assume exponential distribution is the best fit
% assumption is based on graphical analysis
load('TotalDraft.mat');        % load the combined draft data
%----------------------%
% from the statistics for the analyzed exponential distribution:
mu = 2.51418;
var = 6.32111;
big = max(TotalDraft');
%----------------------%

% Set the size of the frame for the meshgrid (user defined)
% ----------
% Since the goal of the project is to simulate a 1 km by 1 km field of ice
% the x and y axis needs to be 100 by 100, such that the draft measurements 1 m apart
% 1000 m x 1000 m = 1,000,000 m

xaxis = 1000; % m
yaxis = 1000; % m

% based on size, evenly distribute markers on axis
% x = [0:1:xaxis-1];
% y = x;
% [x,y] = meshgrid(x);

% based on size of frame, get a distribution of elevations
z1 = exprnd(mu,[length(x),length(y)]);
zmean = mean(mean(z1'));
```

create the txtfile for ArcGis

```
% ------------------------------------------------------------------
% preallocate a matrix
% ------------------------------------------------------------------
Z1 = zeros(numel(z1),5);

          % numel returns the number of elements in elevation matrix z1

% ------------------------------------------------------------------
% This section allocates the column identifier for the final matrix
% ------------------------------------------------------------------
count = 0;
for i = 1:xaxis
    min = count*xaxis+1;        % lower matrix limit
    max = (count+1)*xaxis;      % upper matrix limit
   for j = 1:length(Z1)
      if min<=j && j<= max
```

```
            Z1(j,1) = i;
        end
    end
 count = count + 1;
end
% ------------------------------------------------------------------
% This section allocates the row identifier and the elevation
% for the final matrix
% ------------------------------------------------------------------
count = 0;
k = 1;
for j = 1:xaxis            % let i = 12
     min = count*xaxis+1;         % min = 0
     max = (count+1)*xaxis;     % max = 20
    for i = 1:length(Z1)
        Z1(i,5)= exprnd(mu);
     if min<=i && i<= max
          Z1(i,2)=k;
          k = k+1;
     else
         k = 1;
     end
    end
    count = count + 1;


%-------------------------------------------------------------------
% this creates the degree decimal lat and lon for ArcGis
% and is based off of the 'Site A' lat/lon of 70d22.034'N/145d59.816W
% which becomes 70.36723 N/ 145.9969 W
%-------------------------------------------------------------------
    for l = 1:length(Z1)
        lat = 70.36723;
        Z1(l,3)=lat+((1/27)*Z1(l,1));
        lon = 145.9969;
        Z1(l,4)=lon+((1/127)*Z1(l,2));
    end

end

% load data to an excel file for export
filename = 'ThesisDraftOutput10292019.xlsx';

xlswrite(filename,Z1)
```

Appendix F

ArcGIS Data

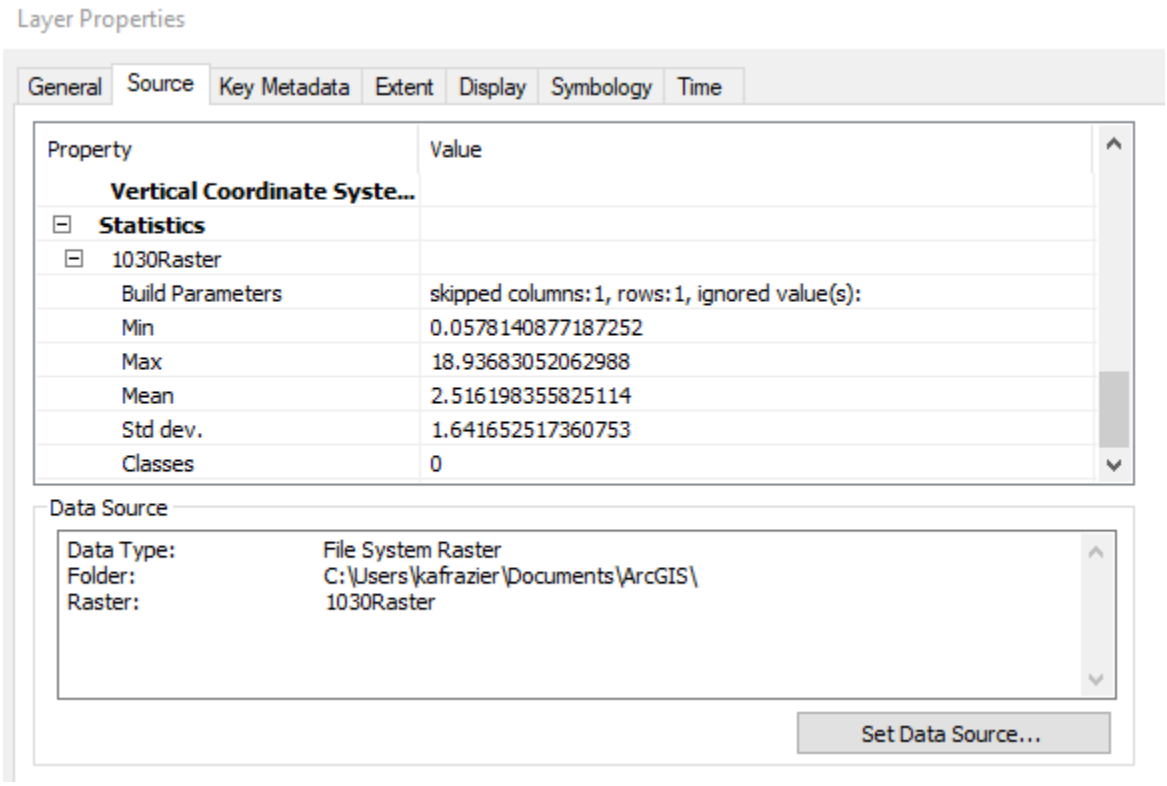

Extent

West -180.000000 **East** 640.000000

North 1000.000000 **South** 1.000000

Date of Run	Raster Area (m2)	Volume (m3)	Depth (m)	Mean Depth (m)
31-Oct	819180	340771.4	0.415991	2.51
8-Nov	819180	281094.1	0.343141	
8-Nov	819180	52675.14	0.064302	1.65

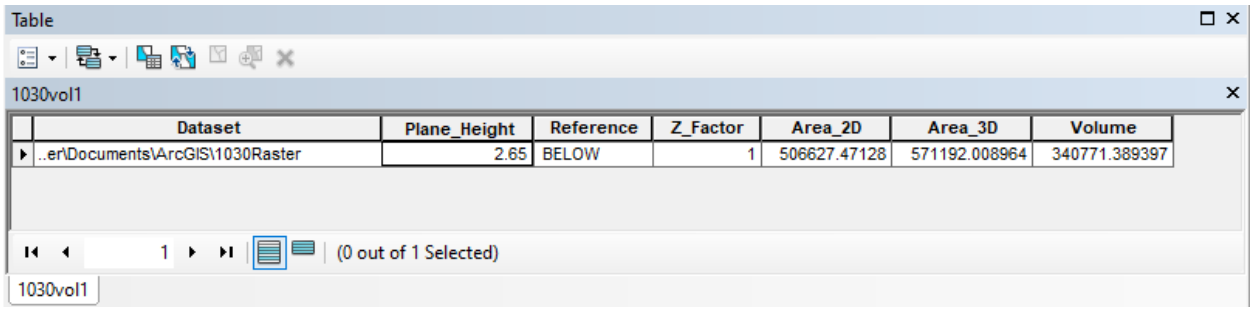
Table
1030vol1
Dataset
Plane_Height
Reference
Z_Factor
Area_2D
Area_3D
Volume
..er\Documents\ArcGIS\1030Raster
2.65
BELOW
1
506627.47128
571192.008964
340771.389397
1
(0 out of 1 Selected)
1030vol1

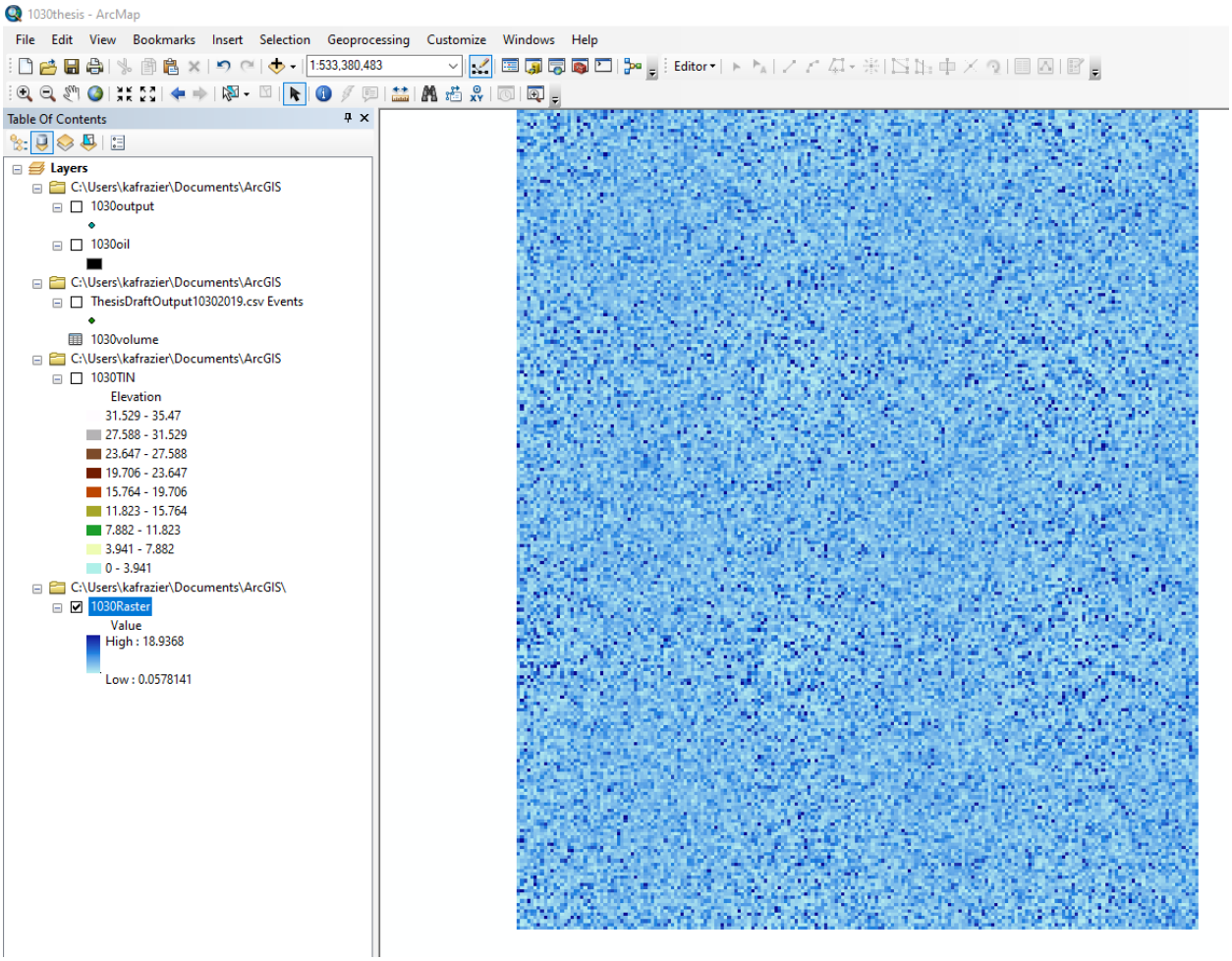
1030thesis - ArcMap
File Edit View Bookmarks Insert Selection Geoprocessing Customize Windows Help
1:533,380,483
Editor
Table Of Contents
Layers
C:\Users\kafrazier\Documents\ArcGIS
1030output
1030oil
C:\Users\kafrazier\Documents\ArcGIS
ThesisDraftOutput10302019.csv Events
1030volume
C:\Users\kafrazier\Documents\ArcGIS
1030TIN
Elevation
31.529 - 35.47
27.588 - 31.529
23.647 - 27.588
19.706 - 23.647
15.764 - 19.706
11.823 - 15.764
7.882 - 11.823
3.941 - 7.882
0 - 3.941
C:\Users\kafrazier\Documents\ArcGIS\
1030Raster
Value
High : 18.9368
Low : 0.0578141

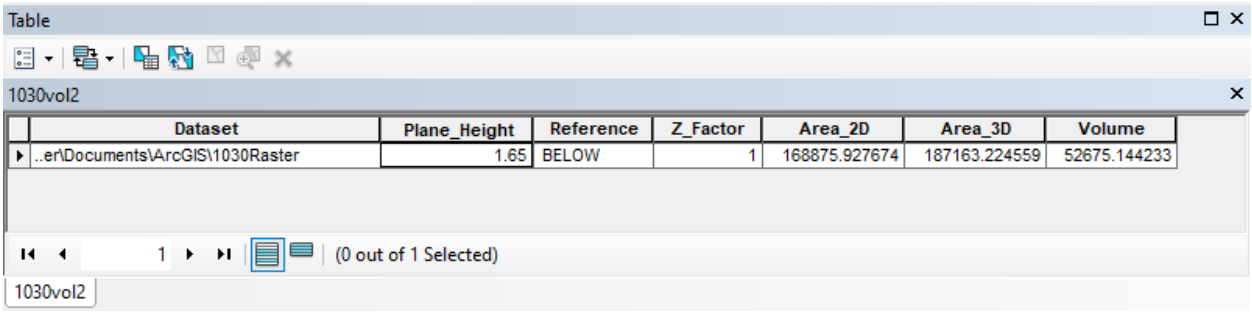
Table
1030vol2
Dataset
Plane_Height
Reference
Z_Factor
Area_2D
Area_3D
Volume
..er\Documents\ArcGIS\1030Raster
1.65
BELOW
1
168875.927674
187163.224559
52675.144233
1
(0 out of 1 Selected)
1030vol2

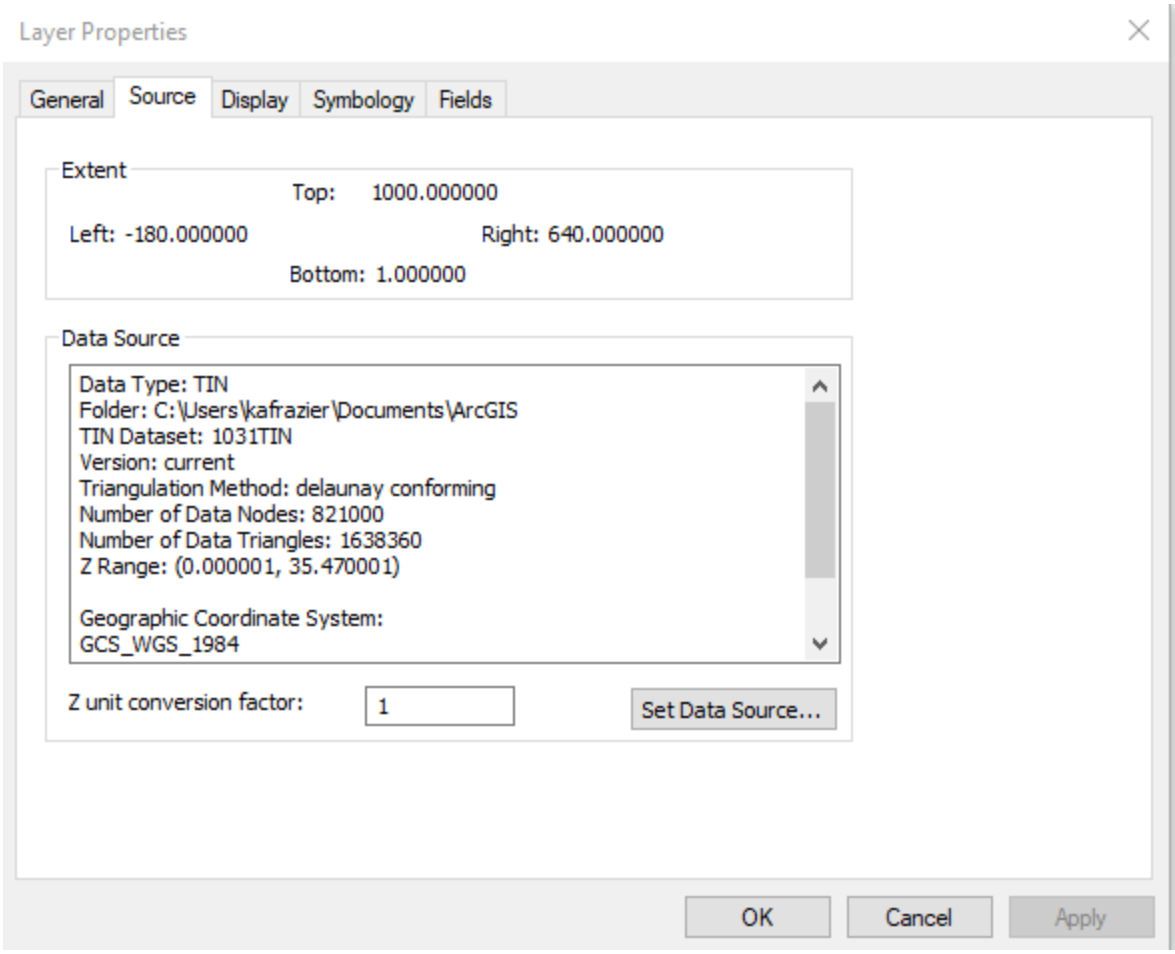
Layer Properties
General
Source
Display
Symbology
Fields
Extent
Top: 1000.000000
Left: -180.000000
Right: 640.000000
Bottom: 1.000000
Data Source
Data Type: TIN
Folder: C:\Users\kafrazier\Documents\ArcGIS
TIN Dataset: 1031TIN
Version: current
Triangulation Method: delaunay conforming
Number of Data Nodes: 821000
Number of Data Triangles: 1638360
Z Range: (0.000001, 35.470001)
Geographic Coordinate System:
GCS_WGS_1984
Z unit conversion factor:
1
Set Data Source...
OK
Cancel
Apply

Table

11volume

Dataset	Plane_Height	Reference	Z_Factor	Area_2D	Area_3D	Volume
..zier\Documents\ArcGIS\11Raster	2.51	BELOW	1	550353.799625	606492.655613	529967.42071

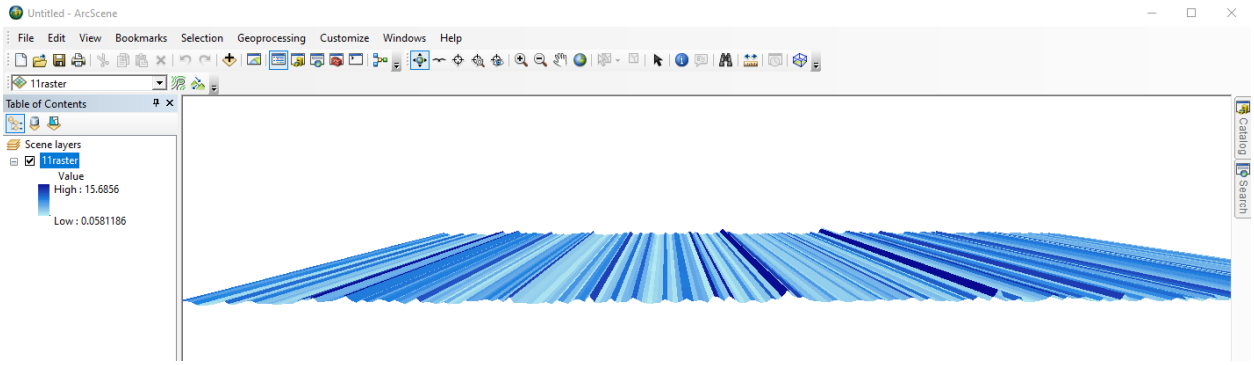

Layer Properties

General | Source | Key Metadata | Extent | Display | Symbology | Time

You can specify the geographic extent of this layer's data source that will be represented by this layer

Set the extent to: the current setting of this layer

Visible Extent

Left: 1

Top: 1000

Bottom: 1.0000000000209

Right: 999.99999999997

Full Extent

(•) of this layer ( ) of the data frame

Left: 1

Top: 1000

Bottom: 1.0000000000209

Right: 999.99999999997

OK Cancel Apply

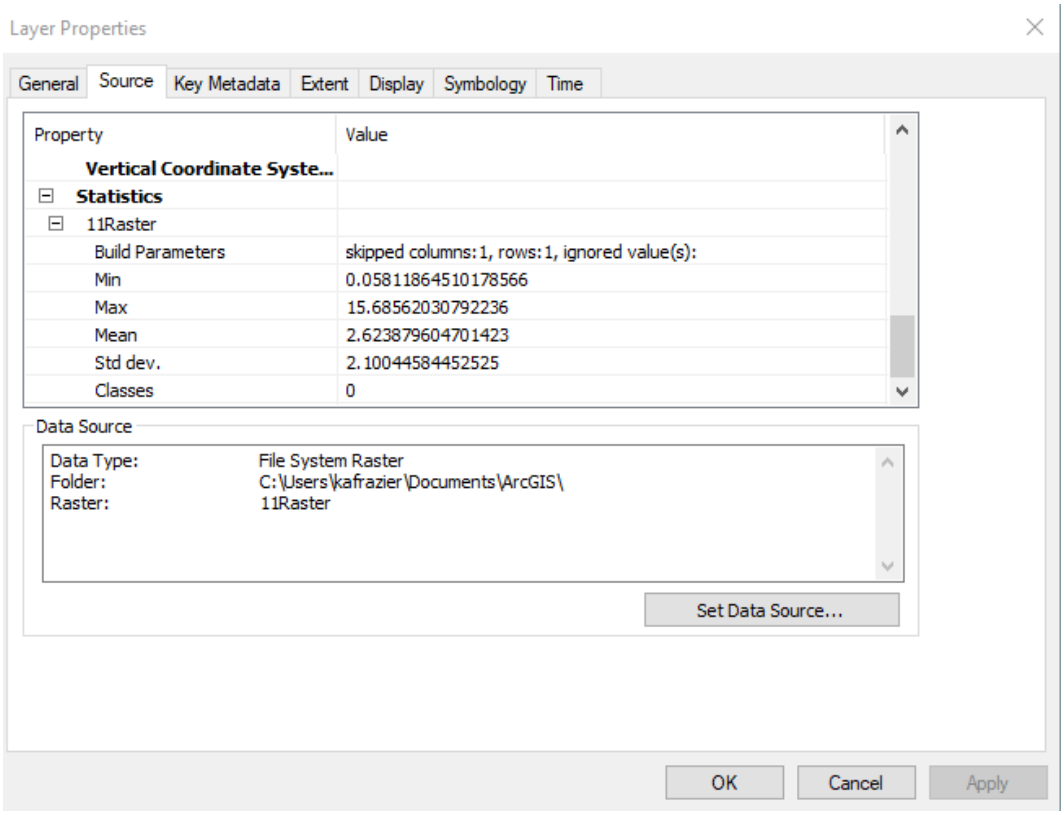
Layer Properties
General
Source
Key Metadata
Extent
Display
Symbology
Time
Property
Value
Vertical Coordinate Syste...
Statistics
11Raster
Build Parameters
skipped columns:1, rows:1, ignored value(s):
Min
0.05811864510178566
Max
15.68562030792236
Mean
2.623879604701423
Std dev.
2.10044584452525
Classes
0
Data Source
Data Type:
File System Raster
Folder:
C:\Users\kafrazier\Documents\ArcGIS\
Raster:
11Raster
Set Data Source...
OK
Cancel
Apply

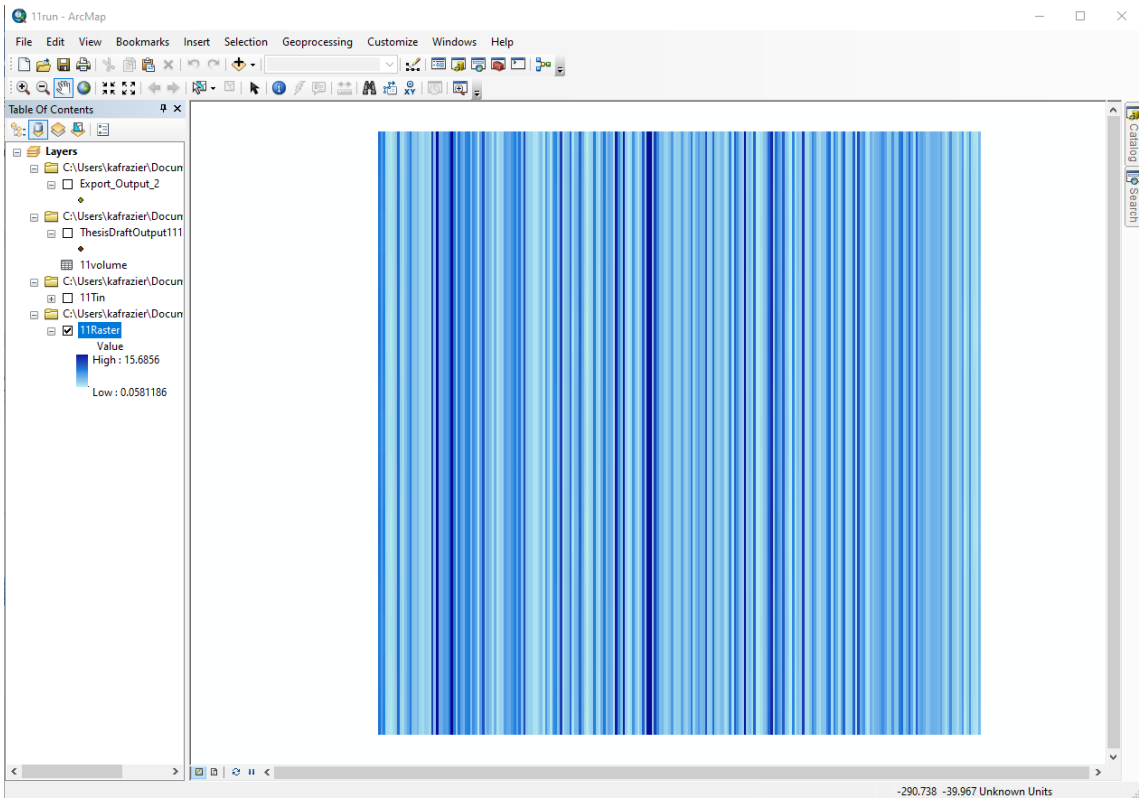
11run - ArcMap
File
Edit
View
Bookmarks
Insert
Selection
Geoprocessing
Customize
Windows
Help
Table Of Contents
Layers
Export_Output_2
ThesisDraftOutput111
11volume
11Tin
11Raster
Value
High : 15.6856
Low : 0.0581186
Catalog
Search
-290.738 -39.967 Unknown Units